

Physical effects involved in the measurements of neutrino masses with future cosmological data

Maria Archidiacono,¹ Thejs Brinckmann,¹ Julien Lesgourgues¹
and Vivian Poulin^{1,2}

¹Institute for Theoretical Particle Physics and Cosmology (TTK),
RWTH Aachen University, D-52056 Aachen, Germany.

²LAPTh, Université Savoie Mont Blanc & CNRS, BP 110,
F-74941 Annecy-le-Vieux Cedex, France.

Abstract. Future Cosmic Microwave Background experiments together with upcoming galaxy and 21-cm surveys will provide extremely accurate measurements of different cosmological observables located at different epochs of the cosmic history. The new data will be able to constrain the neutrino mass sum with the best precision ever. In order to exploit the complementarity of the different redshift probes, a deep understanding of the physical effects driving the impact of massive neutrinos on CMB and large scale structures is required. The goal of this work is to describe these effects, assuming a summed neutrino mass close to its minimum allowed value. We find that parameter degeneracies can be removed by appropriate combinations, leading to robust and model independent constraints. A joint forecast of the sensitivity of Euclid and DESI surveys together with a CORE-like CMB experiment leads to a 1σ uncertainty of 7 meV on the summed neutrino mass. However this particular combination gives rise to a peculiar degeneracy between M_ν and the optical depth at reionization. Independent constraints from 21-cm surveys can break this degeneracy and decrease the 1σ uncertainty down to 5 meV.

Contents

1	Introduction	1
2	Effect of a small neutrino mass on the CMB	3
2.1	General parameter degeneracies for CMB data	3
2.2	CMB data definition	4
2.3	Degeneracies between very small M_ν 's and other parameters with CMB data only	5
3	Effect of neutrino mass on the BAO scale	10
4	Effect of neutrino mass on Large Scale Structure observables	14
4.1	Cosmic shear and galaxy clustering spectrum	14
4.2	Degeneracies between M_ν and other parameters	16
5	Joint Analysis Results	21
5.1	Combination of CMB, BAO and galaxy shear/correlation data	21
5.2	Adding 21cm surveys	23
6	Conclusions	24

1 Introduction

A wide program of future cosmological experiments is planned or proposed, in order not only to pin down cosmological parameters, but also to shed light on fundamental physics related to cosmology. These cosmological experiments include high precision galaxy redshift surveys, such as Euclid, DESI, WFIRST (see [30] and references therein), high precision cosmic shear surveys, such as Euclid and LSST, and finally Cosmic Microwave Background experiments aimed at more accurate polarization measurements, such as CORE [18, 25, 26] and CMB-Stage IV [4, 38].

However, besides experimental sensitivity, parameter constraints are limited by degeneracies: a degeneracy indicates the ability of one parameter to mimic the effect of another parameter on a particular observable, making it impossible to disentangle them and to corner the value of each parameter separately. The key approach to tackle this problem consists in a joint analysis of complementary probes with different degeneracy directions in parameter space. For that reason, the next step in the era of precision cosmology will be based on the synergy of high- and low- redshift probes.

One of the parameters that will benefit from such an approach is the neutrino mass sum (hereafter M_ν). Indeed the impact of massive neutrinos on cosmological observables comes from a very special effect: light massive neutrinos behave as radiation before their non-relativistic transition, while afterwards they gradually become a matter component; therefore their impact on cosmological probes at different redshifts is closely related to their mass.

The neutrino mass effects have been widely studied in the literature [11, 36, 43, 44] and their impact on CMB and large scale structures on linear scales is well known. Even on

non-linear scale, the neutrino mass effect is better understood thanks to recent progress in N-body simulations [3, 16, 19, 20].

However, neutrino cosmology is about to face a revolution for two reasons.

First of all, current upper bounds on the neutrino mass sum are getting closer and closer to the minimum value allowed by the inverted hierarchy $M_\nu \sim 0.11$ eV [2, 23, 51]. Thus, future experiments will look at ultra-light neutrinos that became non-relativistic in a relatively recent cosmological epoch. Very small neutrino masses will have a different effect on the cosmological evolution and, thus, a different impact on cosmological observables. For instance, even if the majority of neutrinos with $m_\nu \leq 600$ meV go non-relativistic after photon decoupling, a small number of them (contributing to the low momentum tail of the phase space distribution) are already partially non-relativistic at decoupling. For $m_\nu \sim 300$ meV this could still have small effects, but not for $m_\nu \sim 60$ meV. Similarly, neutrinos becoming relativistic soon after photon decoupling can produce a distortion of the CMB temperature spectrum through the early Integrated Sachs-Wolfe effect, but again this can only be significant for masses of a few hundreds of meV. Instead, the neutrinos studied in this paper could have individual masses of at most 100 meV.

Secondly future galaxy surveys will reach a very high sensitivity on very small scales. As for now, the use of small scale data is limited by the uncertainty on non linear structure formation, which is difficult to model, especially in presence of massive neutrinos [7, 22, 29, 31]. A major theoretical goal in the next few years will be to provide a better understanding of the processes governing clustering on small scales. Having the non linear effects under control, we will be able to exploit small scale data in order to break degeneracies. The neutrino mass effects are already important on linear scales, but by including smaller and smaller scales one would have a better lever arm and improve the constraints on M_ν .

The aim of this work is to investigate the physical effects induced by massive neutrinos as they will be unveiled by future cosmological data.

We will pay specific attention to the correlation between M_ν and other cosmological parameters, and show that directions of degeneracy are very sensitive to probes of the cosmic history at different epochs. For some combinations of CMB and Large Scale Structure data sets, a correlation between M_ν and τ_{reio} has already been observed in references [4, 47], but its interpretation is far from obvious and requires a detailed investigation. This correlation is very important, for the reason that independent measurements of the optical depth by 21cm surveys will lead to a remarkable improvement on the sensitivity to the neutrino mass [47]. We will confirm this expectation with a dedicated forecast showing that even the minimum allowed value of the summed neutrino mass could be detected at the 10σ level in a time scale of about ten years.

The paper is organized as follows: In section 2, 3 and 4 we study in detail the effect of a variation of the summed neutrino mass in CMB, Baryonic Acoustic Oscillation (BAO) and Large Scale Structure (LSS) observables, respectively. In particular we will carefully describe and explain the degeneracies with other relevant cosmological parameters. In section 5 we will present the results of our Markov Chain Monte Carlo forecast of the sensitivity of future CMB, BAO, LSS and 21cm experiments. Finally in section 6 we will draw our conclusions.

2 Effect of a small neutrino mass on the CMB

2.1 General parameter degeneracies for CMB data

In the minimal, flat, 6-parameter Λ CDM model, it is well-known that the CMB temperature and polarisation unlensed spectra are determined by a number of effects¹, which remain identical as long as one fixes quantities usually depending on distance ratios or density ratios, such as:

- the sound horizon angular scale $\theta_s(z_{\text{dec}}) = \frac{d_s(z_{\text{dec}})}{d_A(z_{\text{dec}})}$ at decoupling,
- the diffusion angular scale $\theta_d(z_{\text{dec}}) = \frac{d_d(z_{\text{dec}})}{d_A(z_{\text{dec}})}$ at decoupling,
- the baryon-to-photon ratio $R_{\text{dec}} = \frac{3\rho_b}{4\rho_\gamma} \Big|_{\text{dec}}$ at decoupling,
- the redshift of radiation-to-matter equality $z_{\text{eq}} = \frac{\rho_m^0}{\rho_r^0} - 1$,
- the redshift of matter-to-cosmological-constant equality $z_\Lambda = \left(\frac{\rho_\Lambda^0}{\rho_r^0}\right)^{1/3} - 1$.

The CMB spectra also depend on a few extra parameters, like the scalar amplitude and tilt (A_s, n_s) and the optical depth at reionization τ_{reio} . However, bearing in mind that the small- ℓ (large angular) part of the spectra is loosely constrained due to cosmic variance, the parameters z_Λ , A_s and τ_{reio} are always less constrained by CMB data than $(\theta_s, \theta_d, R, z_{\text{eq}}, n_s)$, and also than the combination $A_s e^{-2\tau_{\text{reio}}}$ giving the overall spectrum normalisation on small angular scales. The fact that we actually measure lensed CMB spectra gives extra information on the amplitude and slope of the matter power spectrum $P(k, z)$ at low redshift: in practise, this increases the sensitivity to the parameters (A_s, z_Λ) , which enter into the normalisation of $P(k, z)$.

Adding neutrino masses into the model leads to several new effects studied extensively in the literature [39, 40, 43]:

- (a) Neutrino masses affects the background expansion history. If we rely on standard assumptions for the photon and background densities ($T_{\text{cmb}} = 2.726$ K, $N_{\text{eff}} = 3.046$) and further fix ω_b and ω_{cdm} , the changes in the background evolution caused by neutrino masses are confined to late times. Then, the values of $d_s(z_{\text{dec}})$, $d_d(z_{\text{dec}})$, R_{dec} and z_{eq} are preserved, and the neutrino masses only impacts the angular diameter distance (and therefore, θ_s and θ_d in an equal way) and z_Λ (and hence, the loosely constrained late ISW effect). It is even possible to choose an appropriate value of the cosmological constant for each set of neutrino masses, in order to keep a fixed $d_A(z_{\text{dec}})$: in that case, the impact of neutrino masses on the background is confined to variations of z_Λ and of the late ISW effect, and cannot be probed accurately due to cosmic variance, unless external non-CMB datasets come into play.
- (b) At the perturbation level, massive neutrinos interact gravitationally with other species and produce small distortions in the CMB peaks. For individual neutrino masses m_ν smaller than ~ 60 meV, the neutrinos become non-relativistic after recombination: in that case the distortions can only be caused by the early ISW effect, and affect the

¹For a review of these effects, see e.g. [41], section 5.1 of [43], and [40].

CMB temperature spectrum in the multipole range $50 < \ell < 200$ [39, 43, 44]. Note that this neutrino-mass-induced early ISW effect takes place even if the redshift of equality is kept fixed: it is different from the redshift-of-equality-induced early ISW effect, which affects the height of the first CMB peak in the range $100 < \ell < 300$.

- (c) Finally, at the lensing level, massive neutrinos slow down the growth of small-scale structure (leading to the well-known suppression factor $1 - 8\omega_\nu/\omega_m$ in the small-scale matter power spectrum at redshift zero) and globally decrease the impact of CMB lensing: the peaks are less smoothed and the damping tail less suppressed [46].

All these effects have played a role in previous constraints on neutrino masses from CMB data alone, or combined with other probes. Interestingly, while the sensitivity of CMB instruments increases with time, different effects come to dominate the neutrino mass constraints: early ISW effects (b) with WMAP alone [37], lensing effects (c) with Planck alone [1], and background effects (a) when combining CMB data with direct measurements of H_0 [55]. There are now several combinations of cosmological probes giving a 95%CL upper bound on the summed mass $M_\nu \equiv \sum m_\nu$ of the order of 120 meV to 150 meV [2, 23, 32, 51], while neutrino oscillation data enforces $M_\nu \geq 60$ meV at 95%CL [33]. The remaining conservatively allowed window is so narrow, $\Delta M_\nu \sim 90$ meV, that the impact of a realistic variation of the neutrino masses on the CMB is getting really small. Our purpose in section 2.3 is to study precisely this impact, and to understand the degeneracy between M_ν and other parameters when using future CMB data only, specifically for the very low mass range $60 \text{ meV} < M_\nu < 150 \text{ meV}$. This requires some preliminary remarks in section 2.2.

2.2 CMB data definition

The discussion of degeneracies is meaningless unless we specify which data set, and which experimental sensitivities, we are referring to. In this paper, we take as a typical example of future CMB data a next-generation CMB satellite similar to the project CORe+, submitted to ESA for the call M4. A new version of CORe was recently submitted again for the call M5 [25, 26], with a small reduction of the instrumental performances, mainly in angular resolution. However, CORe+ and CORe-M5 are very similar, and the conclusions of this paper would not change significantly by adopting the CORe-M5 settings.

When displaying binned errors in C_ℓ plots, and when doing MCMC forecasts with mock data and synthetic likelihoods, we assume that this CORe-like experiment is based on 9 frequency channels with sensitivity and beam angles given in footnote². We mimic the effect of sky masking by adopting a Gaussian likelihood with an overall rescaling by a sky fraction $f_{\text{sky}} = 0.70$.

Our dataset consists primarily of temperature and E-mode polarisation auto-correlation and cross-correlation spectra $C_\ell^{TT}, C_\ell^{EE}, C_\ell^{TE}$. To get more information on CMB lensing, one can either analyse B-mode maps (in absence of significant primordial gravitational waves, the B-mode only comes from CMB lensing and foregrounds) and add the C_ℓ^{BB} spectrum to the list of observables; or perform lensing extraction with a quadratic or optimal estimator [48], and add the CMB lensing potential spectrum $C_\ell^{\phi\phi}$ to the list of observables (equivalently one could use the deflection spectrum $C_\ell^{dd} = \ell(\ell + 1)C_\ell^{\phi\phi}$). We cannot use both C_ℓ^{BB} and

² Assumed specifications for a CORe+ - like experiment: frequencies in GHz: [100, 115, 130, 145, 160, 175, 195, 220, 255]; θ_{fwhm} in arcmin: [8.4, 7.3, 6.46, 5.79, 5.25, 4.8, 4.31, 3.82, 3.29]; temperature sensitivity in [μK arcmin] : [6.0, 5.0, 4.2, 3.6, 3.8, 3.8, 3.8, 5.8, 8.9]; polarisation sensitivity in [μK arcmin] : [8.5, 7.0, 5.9, 5.0, 5.4, 5.3, 5.3, 8.1, 12.6].

$C_\ell^{\phi\phi}$ in the likelihood: the same information would be counted twice. Here we choose to use the lensing potential spectrum, which better separates the contribution of different scales to lensing, that would be mixed in the C_ℓ^{BB} spectrum by some integration kernel. To give an example, we will see in Figure 1 (bottom plots) that the neutrino mass effect on $C_\ell^{\phi\phi}$ is more pronounced on small angular scales, while in the lensed C_ℓ^{BB} this effect would be nearly independent of ℓ^3 .

So the CMB data set that we have in mind consists in measurements for $C_\ell^{TT}, C_\ell^{EE}, C_\ell^{TE}, C_\ell^{\phi\phi}$, with a synthetic Gaussian likelihood similar to that in [53], and a lensing extraction error spectrum $N_\ell^{\phi\phi}$ based on the quadratic estimator method [50] for the EB estimator. In the likelihood, we keep the lensed $C_\ell^{TT}, C_\ell^{EE}, C_\ell^{TE}$. Indeed, unlike C_ℓ^{BB} , these spectra are only weakly affected by lensing, and the lensing information redundancy between lensed temperature/polarisation spectra and the $C_\ell^{\phi\phi}$ spectrum is small enough for being negligible at the instrumental sensitivity level of a CORE-like experiment [24].

2.3 Degeneracies between very small M_ν 's and other parameters with CMB data only

We will discuss the impact of increasing the neutrino mass, while keeping various parameters or combination of parameters fixed. We illustrate this discussion with the plots of Figure 1, showing the spectrum ratio between different models sharing a summed mass $M_\nu = 150$ meV and a baseline model⁴ with $M_\nu = 60$ meV. The plots show the residuals of the lensed TT (top), lensed EE (middle) and lensing potential (bottom) power spectrum, as a function of multipoles ℓ with a linear (left) or logarithmic (right) scale. The light/pink and darker/green shaded rectangles refer respectively to the binned noise spectrum of a cosmic-variance-limited or CORE-like experiment, with linear bins of width $\Delta\ell = 25$. All spectra are computed with the Boltzmann solver CLASS⁵ [17, 42, 45], version 2.5.0, with the high precision settings `cl_permille.pre`.

Our discussion will also be illustrated by the results of Monte Carlo Markov Chains (MCMC) forecasts for our CORE-like experiment: Figure 2 gives the 2D probability contours for the pairs of parameters most relevant to our discussion. The MCMC forecasts are done with the MONTEPYTHON package⁶ [8].

The main conclusions can be reached in four steps:

³However, we will also see that *within the range in which error bars are small*, the neutrino mass effect on $C_\ell^{\phi\phi}$ is also *nearly* ℓ -independent, so we may expect that trading $C_\ell^{\phi\phi}$ against C_ℓ^{BB} in the likelihood would have a minor impact on our conclusions.

⁴Our discussion is general and the value of cosmological parameters for the baseline model is unimportant. We choose Planck-inspired values, $\{\omega_b, \omega_{\text{cdm}}, h, n_s, A_s, \tau_{\text{reio}}, M_\nu\} = \{0.02214, 0.12070, 0.6688, 0.9624, 2.12 \times 10^{-9}, 0.0581, 0.06 \text{ eV}\}$, giving an angular sound horizon at recombination θ_s (which defines the angular scale of the CMB acoustic peaks) roughly equal to $100 \theta_s = 1.0415$. In this work, our total neutrino mass M_ν is assumed to be shared equally among the three species, like in the degenerate (DEG) model. This choice is not random: it is motivated by the fact that the cosmological impact of different mass splittings is negligible, at least as long as one compares some DEG, NH (Normal Hierarchy) and IH (Inverted Hierarchy) models all sharing the same total mass M_ν . This is not necessarily true when comparing them with a model with “one massive, two massless neutrinos”, which departs by a much larger amount at the level of the matter power spectrum [43, 44]. Hence, by varying the mass M_ν of the DEG model, we obtain results which apply at the same time, in very good approximation, to the two realistic cases NH and IH.

⁵<http://class-code.net>

⁶<http://baudren.github.io/montepython.html>

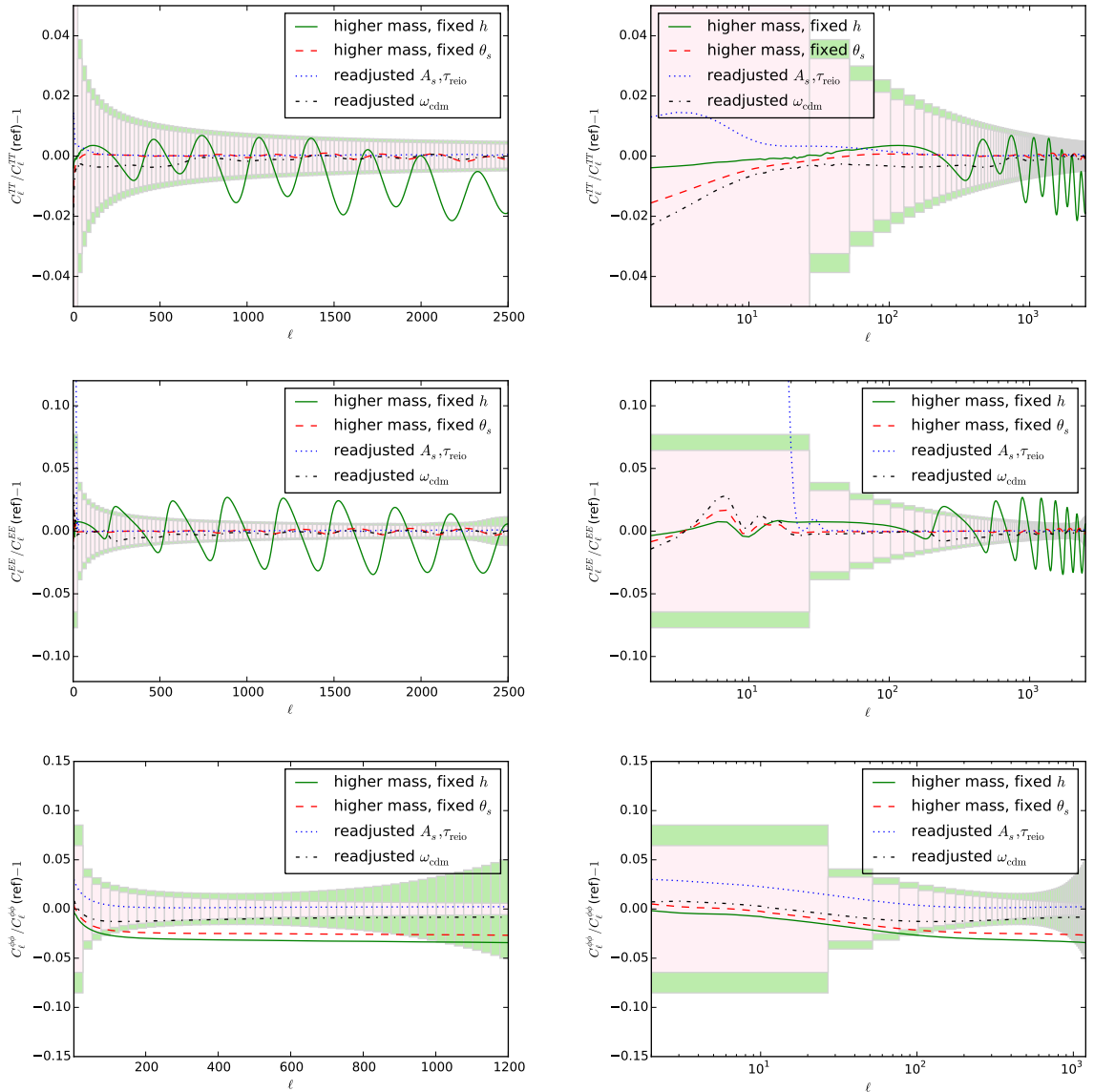


Figure 1. Relative change in the CMB spectra induced by increasing the summed neutrino mass from $M_\nu = 60$ meV to $M_\nu = 150$ meV. The plots show the residuals of the lensed TT (top), lensed EE (middle) and lensing potential (bottom) power spectrum, as a function of multipoles ℓ with a linear (left) or logarithmic (right) scale. The light/pink and darker/green shaded rectangles refer, respectively, to the binned noise spectrum of a cosmic-variance-limited or CORE-like experiment, with linear bins of width $\Delta\ell = 25$. The physical baryon density ω_b and the scalar spectral index n_s are kept fixed. In the first case (green solid line) the value of the Hubble constant is fixed at the reference value, while in all the other cases (labeled as fixed θ_s) h decreases in order to keep θ_s consistent with the reference model. Moreover, in the third case (dotted blue line), we tried to compensate for the changes in the lensing spectrum by increasing A_s , and in the fourth case (dotted-dashed black) we aim at the same result by increasing ω_{cdm} .

1. We first assume that we increase neutrino masses with respect to the baseline model, while keeping the parameters $\{\omega_b, \omega_{\text{cdm}}, h, n_s, A_s, \tau_{\text{reio}}\}$ fixed (green solid curve in Figure 1). Given the discussion in point (a), we expect that this is not a very clever choice,

because the angular diameter distance is not preserved. So if the baseline model is a good fit to the data, the new model will be discrepant. Indeed, by looking especially at the top left and middle left plots in Figure 1, we see even-spaced oscillations signalling a change in the angular diameter distance, and the residuals are far above the instrumental noise.

2. We then perform the same increase in M_ν , but now with a fixed angular diameter distance to recombination, which means that $\{\omega_b, \omega_{\text{cdm}}\}$ are still fixed, but h varies. With CLASS, this is easily achieved by keeping the input parameter $100\theta_s$ constant. Since the early cosmology and the sound horizon at decoupling are fixed, fixing θ_s means adjusting H_0 and the angular diameter distance for each M_ν . Then, the angular diffusion scale θ_d is also automatically fixed. In Figure 1, this transformation corresponds to the dashed red residuals. As expected, the previous oscillations disappear in the residuals. The only visible effects are much smaller oscillations, some tilt at large ℓ due to a different level of CMB lensing, and a tilt at small ℓ due to a different late ISW effect. However, both effects are below cosmic variance. We conclude that, the measurement of the temperature and E-mode spectra alone does not allow us to distinguish between $M_\nu = 60$ meV and 150 meV, and that in a CMB analysis the parameters (M_ν, H_0) are inevitably correlated, as is well known, and illustrated by the upper left plot in Figure 2.

We can try to quantify this correlation. A simple numerical exercise shows that in order to keep the same value of θ_s while fixing $\{\omega_b, \omega_{\text{cdm}}\}$ and varying M_ν , one finds a correlation

$$\Delta h \simeq -0.09 \left(\frac{\Delta M_\nu}{1 \text{ eV}} \right). \quad (2.1)$$

We will come back to this relation later, and show that the correlation angle changes slightly when other effects are taken into account.

We now look at the bottom plots in Figure 1, showing variations in the lensing potential spectrum. The dashed red line is consistent with the fact that a higher neutrino mass implies more suppression in the small-scale matter power spectrum $P(k, z)$, and hence in the large- ℓ lensing potential spectrum $C_\ell^{\phi\phi}$. A comparison with the instrumental errors show that this effect is potentially relevant: the dashed red residual is outside the 68% error bars in about 30 consecutive bins, leading to a χ^2 increase by many units. It is also visible that the neutrino mass effect would be detectable only in a range given roughly by $50 \leq \ell \leq 800$, in which the effect is nearly equivalent to a suppression by some ℓ -independent factor (by about 3% in our example).

Hence, we see that a CORE-like CMB experiment could in principle discriminate between $M_\nu = 60$ meV and 150 meV, and that the effect of the neutrino mass with fixed $\{\omega_b, \omega_{\text{cdm}}, \theta_s, n_s, A_s, \tau_{\text{reio}}\}$ can be simply summarised as an apparent mismatch between the normalisation of the TT, TE, EE spectra and that of the CMB lensing spectrum. To check whether the distinction can be made in reality, and not just in principle, we must think whether the variation of other cosmological parameters could cancel this effect, and lead to new parameter correlations with M_ν .

As explained in reference [52], in a pure Λ CDM model with no massive neutrinos, the dependence of the global amplitude of $C_\ell^{\phi\phi}$ on the cosmological parameters is given

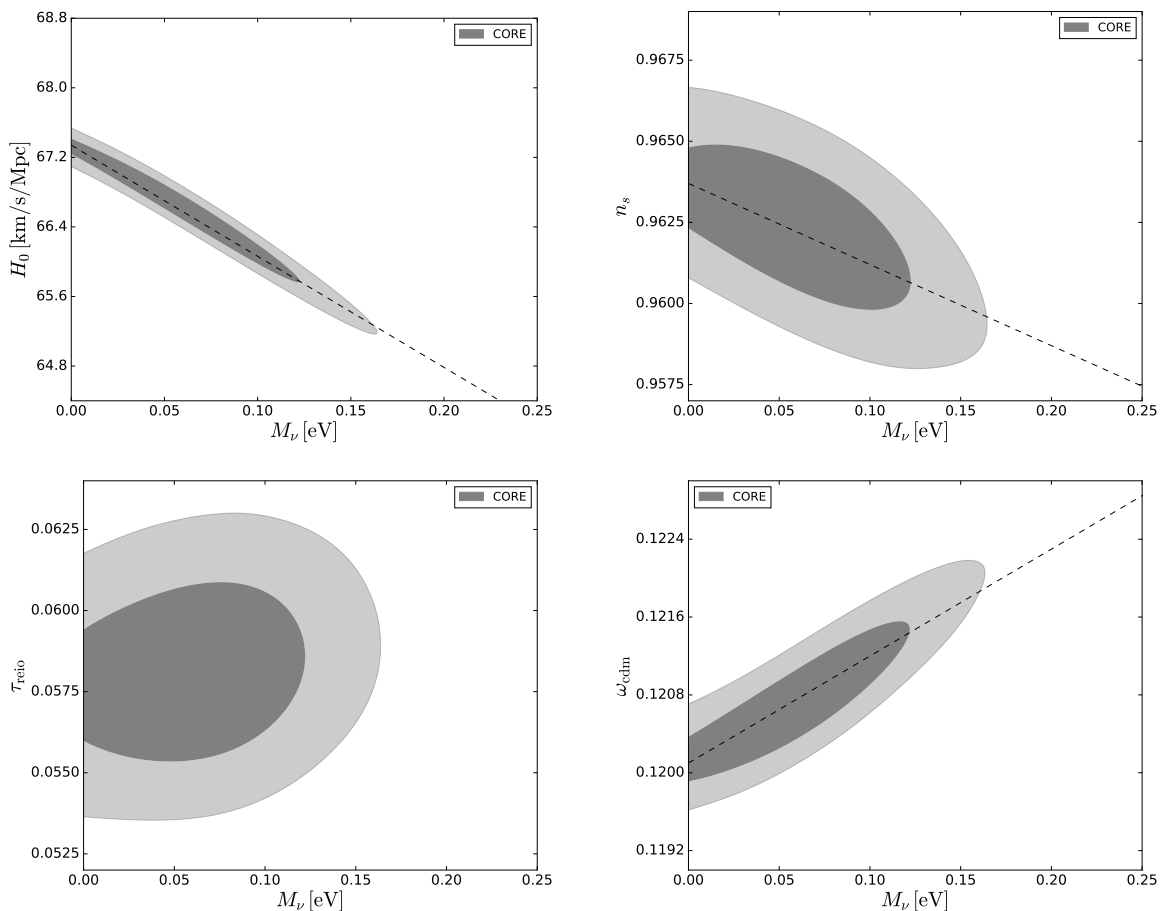


Figure 2. 68% and 95% CL posterior probability contour levels for different pairs of parameters, for an MCMC forecast of the sensitivity of a CORE-like experiment to the parameters of a 7-parameter model (Λ CDM plus total neutrino mass M_ν). The CMB data is assumed to consist of measurements of the TT, EE, TE and lensing potential spectra.

approximately by:

$$\ell^4 C_\ell^{\phi\phi} \propto A_s (\Omega_m^{0.6} h)^{2.5} \quad (\ell > 200),$$

and in terms of ω_m

$$\ell^4 C_\ell^{\phi\phi} \propto A_s \omega_m^{3/2} h^{-1/2} \quad (\ell > 200),$$

plus an additional minor dependence on Ω_m . If we include massive neutrinos, the linear growth of structure becomes scale dependent, thus the exact impact of M_ν on $C_\ell^{\phi\phi}$ is ℓ -dependent, but only by a small amount in the range constrained by observations. Anyway, given that the neutrino mass slows down the growth of cold dark matter perturbations, we can generally assume:

$$\ell^4 C_\ell^{\phi\phi} \propto A_s \omega_m^{3/2} h^{-1/2} M_\nu^{-\alpha}, \quad (2.2)$$

with $\alpha > 0$. This qualitative result shows that in order to compensate an increase of M_ν , we have a priori two possibilities: increasing A_s , or increasing ω_m . We will explore them one after each other in the next points, and arrive at interesting conclusions.

3. We have the possibility to increase A_s in order to compensate for the neutrino mass effect in $C_\ell^{\phi\phi}$, while keeping $A_s e^{-2\tau_{\text{reio}}}$ fixed, in order to have the same overall normalisation of the large- ℓ temperature and polarisation spectra. Hence, this transformation implies a higher reionisation optical depth τ_{reio} . We could expect that, this change in the optical depth is unobservable due to cosmic variance, which would mean that there is a parameter degeneracy at the level of CMB data, and that the three parameters $(M_\nu, A_s, \tau_{\text{reio}})$ are correlated.

This turns out not to be the case. In our example, the higher neutrino mass shifts the lensing potential down by 3%. This could be compensated by increasing A_s by 3% as well, and shifting τ_{reio} by $\Delta\tau_{\text{reio}} = \frac{1}{2} \log 1.03 \simeq 0.015$. This is a very big shift compared to the expected sensitivity of a CORE-like experiment, $\sigma(\tau_{\text{reio}}) \simeq 0.002$. Hence this degeneracy should not be present.

This is illustrated by the third set of curves (dotted blue) in Figure 1. We estimated numerically the reduction factor for $C_{400}^{\phi\phi}$ in the second model (red dashed). We increased A_s by exactly this factor, keeping $A_s e^{-2\tau_{\text{reio}}}$ fixed. The new model has a much larger reionisation bump in C_ℓ^{EE} , with a residual largely exceeding the error bars.

The lower left plot in Figure 2 brings the final confirmation that in a global fit of CMB data, with lensing extraction included, there is no significant correlation between M_ν and τ_{reio} .

At this point, we still expect that very small neutrino masses could be accurately measured by CMB data alone, unless the other way to compensate for the neutrino mass effect in the lensing potential (by increasing ω_m) works better than increasing A_s , and does lead to some parameter degeneracy. This is what we will explore in the final step of this discussion.

4. Considering that ω_b is accurately determined by the first peak ratios, we can increase $\omega_m = \omega_b + \omega_{\text{cdm}}$ by enhancing ω_{cdm} only. It is difficult to infer analytically from equation (2.2) the amount by which ω_{cdm} should be enhanced in order to cancel the effect of M_ν in the lensing potential, because during the transformation, we must keep θ_s fixed; since θ_s depends on both h and ω_m , the Hubble parameter will also change.

In the example displayed in figure 1, we found numerically the factor by which we should increase ω_{cdm} (with fixed ω_b and θ_s), in order to nearly cancel the neutrino mass effect in the lensing power spectrum. This leads to the dotted-dashed black curve. In the lensing potential plots (bottom), the new residual is back inside the cosmic variance band.

The problem with the previous attempt was that changing τ_{reio} had “side effects” (namely, on the reionisation bump) potentially excluded by the data. Increasing ω_{cdm} also has “side effects”: it affects the redshift of radiation/matter equality z_{eq} , and hence the amplitude of the first two peaks (through gravity boost effects and through the early ISW effect); it also affects the redshift of matter/ Λ equality z_Λ and the late ISW effect; and finally, it has a small impact on the angular diameter distance. All these effects can be identified by looking at the details of the dotted-dashed black residuals in figure 1. The key point is that a tiny enhancement of ω_{cdm} is enough to compensate for the neutrino mass effect in $C_\ell^{\phi\phi}$, in such way that the “side effects” all remain well below cosmic variance. Hence, we expect a parameter degeneracy between M_ν and ω_{cdm} when using CMB data alone, that will compromise the accuracy with

which the neutrino mass can be pinned down, and lead to a correlation between these parameters.

This is confirmed by the lower right plot in Figure 2: in a global fit of CMB data, we obtain a degeneracy direction approximately parametrised by the slope of the dashed curve in that plot,

$$\Delta\omega_{\text{cdm}} = 0.01 \Delta M_\nu \sim \Delta\omega_\nu . \quad (2.3)$$

Which is exactly the relation we used in figure 1, when transforming to the fourth model (dotted-dashed black curves).

We can reach the main conclusion of this section: for CMB data alone (including lensing extraction), there is no significant parameter degeneracy between $(M_\nu, A_s, \tau_{\text{reio}})$, but there is one between M_ν and ω_{cdm} . This is the most pronounced parameter degeneracy involving the neutrino mass when the cosmological model is parametrised by $\{\omega_b, \omega_{\text{cdm}}, \theta_s, n_s, A_s, \tau_{\text{reio}}\}$, and the correlation is given approximately by equation (2.3).

If instead the model is parametrised by $\{\omega_b, \omega_{\text{cdm}}, h, n_s, A_s, \tau_{\text{reio}}\}$, for the obvious reasons discussed previously, there is an additional clear correlation between M_ν and h . We return to the correlation factor, that we estimated before to be given by equation (2.1). This equation is actually not a very good fit of the contours in the upper left plot of Figure 2: the dashed line in that plot corresponds to

$$\Delta h \simeq -0.13 \left(\frac{\Delta M_\nu}{1 \text{ eV}} \right) . \quad (2.4)$$

The explanation for this mismatch is simple. Equation (2.1) assumed fixed θ_s and ω_{cdm} values. If instead we try to keep θ_s fixed while varying ω_{cdm} according to equation (2.3), we see increased correlation between M_ν and h , as shown by equation (2.4)⁷.

Hence, with CMB data only, the clearest and most important degeneracies involving the summed neutrino mass are between M_ν and ω_{cdm} (due to lensing) and M_ν and h (due to the angular diameter distance). There are other correlations, but they are much less pronounced. The third one would be between M_ν and n_s . This can be understood by looking closely at the dotted-dashed in figure 1 (lower right plot). The variation of ω_{cdm} did not only rescale the amplitude of the CMB lensing potential, it also generated a small positive tilt. Hence, the $(M_\nu, \omega_{\text{cdm}})$ degeneracy is more pronounced when it goes together with a tiny decrease of the tilt n_s , by such a small amount that it would not conflict with temperature and polarisation data. This negative correlation is visible in Figure 2, upper right plot.

3 Effect of neutrino mass on the BAO scale

The acoustic oscillations of the baryon-photon fluid that we observe in the CMB power spectrum produce a characteristic feature in the two point correlation function. In Fourier space the feature is located at a peculiar scale, the BAO scale, $k_{\text{BAO}} = 2\pi/r_s(z_{\text{drag}})$, where $r_s(z_{\text{drag}})$ is the comoving sound horizon at baryon drag

$$r_s(z_{\text{drag}}) = \int_0^{\tau_{\text{drag}}} c_s d\tau = \int_{z_{\text{drag}}}^{\infty} \frac{c_s}{H(z)} dz.$$

⁷Note that we estimated the correlation factor in equation (2.3) with one significant digit, and in equation (2.4) with two significant digits: this is consistent with the fact that the correlation is much more clear and pronounced in the second case (the ratio of the minor over major axis is much smaller).

The observed scale, assuming an isotropic fit of a galaxy sample⁸, provides the ratio $r_s(z_{\text{drag}})/D_V(z_{\text{BAO}})$, where D_V is the volume distance, defined as

$$D_V(z) = [z/H(z)(1+z)^2 d_A(z)^2]^{1/3},$$

and $D_A = (1+z)d_A(z)$ is the comoving angular diameter distance. In the Λ CDM model with massive neutrinos, the ratio $r_s(z_{\text{drag}})/D_V(z_{\text{BAO}})$ can only depend on the four parameters $\{\omega_b, \omega_{\text{cdm}}, \omega_\nu, h\}$. More precisely, $r_s(z_{\text{drag}})$ depends on the three parameters $\{\omega_b, \omega_{\text{cdm}}, h^2\}$, while for redshifts below the non-relativistic transition, $z \ll z_{\text{nr}} \sim 2 \times 10^3 (m_\nu/1 \text{ eV})$, $D_A(z)$ depends only on $\omega_{\text{tot}} = \omega_b + \omega_{\text{cdm}} + \omega_\nu$ and on h , because it can be approximated as

$$D_A(z) = \int_0^z \frac{cdz'}{H(z')} \simeq 3000 \int_0^z \frac{dz'}{\sqrt{\omega_{\text{tot}}(1+z')^3 + (h^2 - \omega_{\text{tot}})}} \text{ Mpc}. \quad (3.1)$$

Note that the term inside the square root is a polynomial in z' in which the constant term is precisely h^2 (so as expected, for small redshifts $z \ll 1$, $D_A(z)$ depends *only* on the h parameter, like in a Hubble diagram).

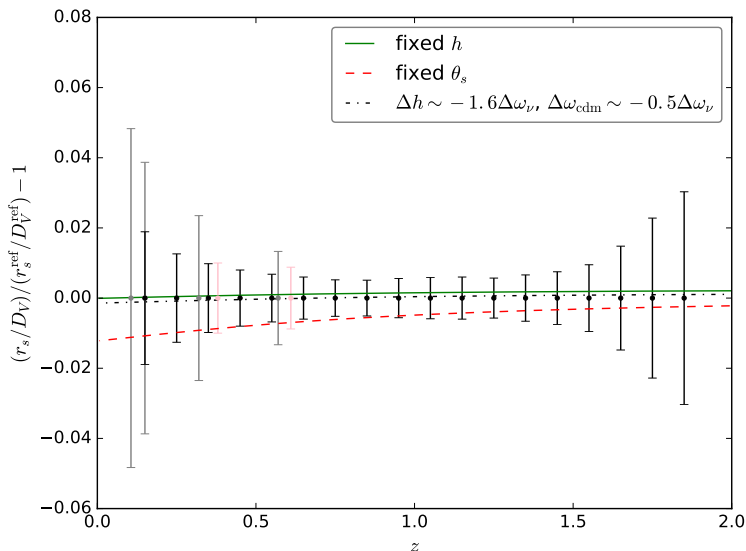


Figure 3. Relative error on r_s/D_V . Gray error bars refer to the current BAO measurements: from left to right 6dFGRS [14], SDSS MGS [56], LOW-Z, C-MASS [5]; the pink error bars are from SDSS-DR12 [15]. Black error bars mark the expected sensitivity of the future DESI experiment [4, 30]. Green solid line and red dashed lines are the same as in figure 1, i.e. higher M_ν with fixed h (green solid line) and higher M_ν with fixed θ_s and varying h (red dashed line). However, here the black dot dashed line is obtained by increasing M_ν and varying h and ω_{cdm} as in equations (3.2).

In figure 3 we show the residuals of current and future BAO measurements, taking as a reference the same model as before with $M_\nu = 60 \text{ meV}$, as well as the relative difference on $r_s(z_{\text{drag}})/D_V(z_{\text{BAO}})$ between several models with a higher mass $M_\nu = 150 \text{ meV}$ (already

⁸Anisotropic fit allow to disentangle the longitudinal information (i.e. the radial scale Hr_s) from the transverse one (i.e. the tangential scale D_A/r_s).

introduced in section 2.3) and the reference model. For future measurement we take the example of DESI, assuming the same sensitivity as in Refs. [4, 30].

We first vary only M_ν with fixed $\{\omega_b, \omega_{\text{cdm}}, h, n_s, A_s, \tau_{\text{reio}}\}$ (green solid line). This means that the early cosmological evolution is identical, while the matter density is slightly enhanced at late times (after the neutrino non-relativistic transition), by about one percent. Thus $d_s(z_{\text{dec}})$ and $r_s(z_{\text{drag}})$ are fixed, but $d_A(z_{\text{dec}})$, $d_A(z_{\text{BAO}})$ and $D_V(z_{\text{BAO}})$ are subject to change. We have seen that this transformation shifted the CMB peaks by a detectable amount. However, the accuracy with which CORE+ will measure θ_s ($< 0.01\%$) is much greater than that with which DESI will measure the BAO angular scales ($\sim 1\%$). From equation 3.1 we can see analytically that the typical variation of $D_A(z)$ between the two models is negligible for $z \ll 1$ and of the order of $\frac{1}{2} \frac{\Delta\omega_\nu}{\omega_{\text{tot}}} \simeq 0.25\%$ for $1 < z < z_{\text{nr}}$. This explains why the green curve in figure 3 remains within the BAO error bars.

This preliminary discussion brings us to the key points of this section:

- *the BAO data alone can bound the neutrino mass, but not with great accuracy.* We showed previously that increasing M_ν with fixed $\{\omega_b, \omega_{\text{cdm}}, h\}$ had no detectable effects, but this was because the mass variation was too small. If one keeps increasing ω_ν with the other parameters fixed, the function inside the square root in equation 3.1 keeps increasing for the same value z' , and $D_A(z)$ decreases. To avoid a BAO bound on M_ν , one could try to exactly compensate the variation $\Delta\omega_\nu$ by an opposite variation in either ω_b or ω_{cdm} , to keep $D_A(z)$ exactly constant. But in that case, the early cosmological evolution would change (sound speed, redshift of equality, redshift of baryon drag) and the ratio $r_s(z_{\text{drag}})/D_V(z_{\text{BAO}})$ would be shifted anyway. Hence there is no parameter degeneracy cancelling exactly the effect of M_ν in BAO observables, at least in the $\Lambda\text{CDM}+M_\nu$ model. This explains why in figures 4 and 5, the contours involving M_ν are closed for DESI data alone, setting an upper bound on the summed mass of a few hundreds of meV.
- *the strong degeneracy between M_ν and h observed in the CMB case cannot exist with BAO data.* This degeneracy came from the possibility to keep constant angular scales ($\theta_s(z_{\text{dec}}), \theta_d(z_{\text{dec}})$) by varying h with fixed $\{\omega_b, \omega_{\text{cdm}}\}$. Indeed, when fitting CMB data with different neutrino masses, one can keep the same value of $d_A(z_{\text{dec}})$ by altering the late time cosmological evolution: while M_ν tends to enhance the density at late times, one can decrease h and the cosmological constant in order to compensate for this effect. This cannot be done with BAO data, because they probe $d_A(z)$ at several small values of z , comparable to the redshift of the transition z_Λ . The proof is particularly obvious if we look at equation 3.1 again. Whatever change in h modifies the constant term inside the square root, and thus the value of $D_A(z)$ for $z \leq 1$. Thus the (M_ν, h) degeneracy discussed in the CMB section must be broken by BAO data. We get a first confirmation of this by looking at the red dashed curve in figure 3, obtained by increasing M_ν with a constant $\theta_s(z_{\text{dec}})$: the new model departs from the other one by a detectable amount, at least given BAO-DESI errors (especially at $z \ll 1$, as expected from this discussion). The second confirmation comes from the right plot in figure 4, showing very different correlations between M_ν and h for CMB-CORE alone and BAO-DESI alone.
- *there exists, however, a correlation between M_ν , h and ω_{cdm} with BAO data, but along different angles than with CMB data.* This comes from the possibility to modify parameters in such a way that both $r_s(z_{\text{drag}})$ and $D_V(z_{\text{BAO}})$ get shifted, but almost by

the same relative amount. To compensate for the effect of an increasing ω_ν , one has three parameters to play with: $\{\omega_b, \omega_{\text{cdm}}, h\}$. However, ω_b is precisely fixed by CMB data alone, and for that reason we keep it to its Planck best-fit value. We then find that variations of the other two parameters by approximately

$$\Delta\omega_{\text{cdm}} \sim -0.5\Delta\omega_\nu, \quad \Delta h \simeq -0.017 \left(\frac{\Delta M_\nu}{1 \text{ eV}} \right) \simeq -1.6 \Delta\omega_\nu \quad (3.2)$$

achieve a nearly constant ratio $r_s(z_{\text{drag}})/D_V(z_{\text{BAO}})$ in the redshift range best probed by the BAO-DESI experiment. As argued before, this ratio is more sensitive to h than ω_{cdm} in that range, so the correlation between ω_{cdm} and ω_ν is weak, while that between h and ω_ν is strong (see Figure 4).

The parameter correlations found in eq. (3.2) for BAO data are very different from those found in the previous section for CMB data:

$$\Delta\omega_{\text{cdm}} \sim \Delta\omega_\nu, \quad \Delta h \simeq -0.13 \left(\frac{\Delta M_\nu}{1 \text{ eV}} \right) \simeq -12 \Delta\omega_\nu. \quad (3.3)$$

The combination of CMB and BAO data can thus break these degeneracies, as is often the case when combining high and low redshift probes of the expansion history. The breaking does not arise from the joint measurement of ω_{cdm} and ω_ν (because BAO data are much less sensitive to ω_{cdm} alone than CMB data), but from that of h and ω_ν , for which the different directions of degeneracy appear very clearly on figure 4. Thus, the future BAO-DESI data will contribute to tighter constraints on M_ν .

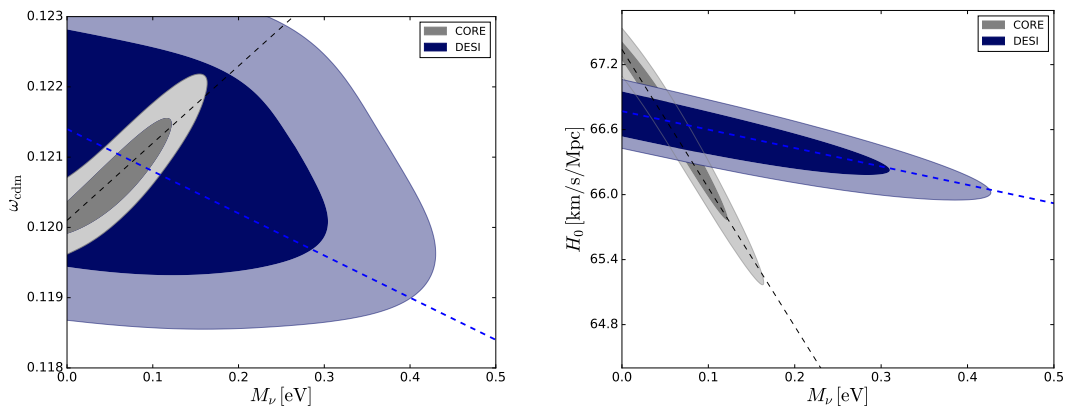


Figure 4. Marginalized one- and two- σ contours in the plane $(\omega_{\text{cdm}}, M_\nu)$ (left panel) and (H_0, M_ν) (right panel), for CMB-CORE or BAO-DESI mock data. The black dashed lines show the directions of degeneracy given in equations (3.3), and the blue ones in equations (3.2).

Another way to illustrate the degeneracies discussed here is to fit CMB data or BAO data alone with a $\Lambda\text{CDM}+M_\nu$ model, and to plot the results in the space of parameters $(M_\nu, \theta_s(z_{\text{dec}}))$ and $(M_\nu, r_s(z_{\text{drag}})/D_V(z_{\text{BAO}}))$ for a median redshift $z_{\text{BAO}} = 1$. This is shown in figure 5. When fitting CMB alone, thanks to the degeneracy of equations (3.3), we can increase M_ν while keeping $d_A(z_{\text{dec}})$ and $\theta_s(z_{\text{dec}})$ fixed (left plot), but this is at the expense of decreasing the BAO angular scale by more than allowed by observational errors (right plot). Conversely, when fitting BAO data alone, we can play with the degeneracy of equations (3.2)

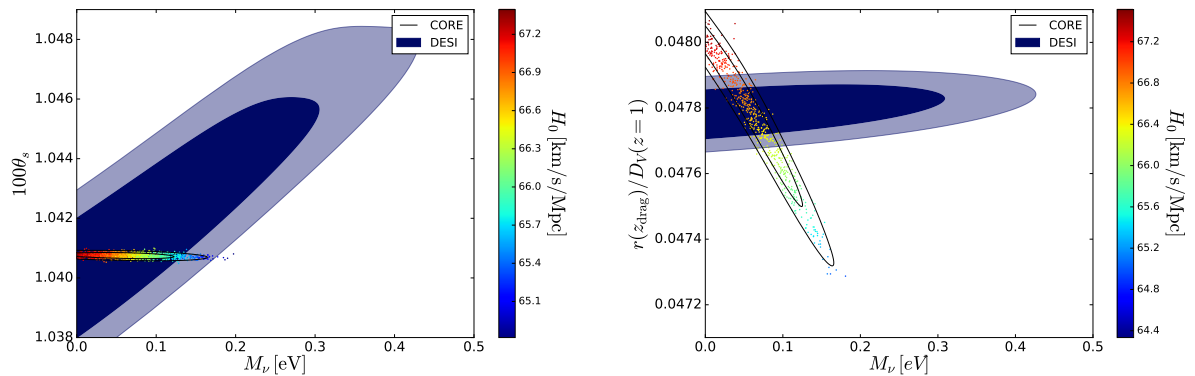


Figure 5. Marginalized one- and two- σ contours in the plane $(\theta_s(z_{\text{dec}}), M_\nu)$ (left) and $(r(z_{\text{drag}})/D_V(z=1), M_\nu)$ (right), for CMB-CORE or BAO-DESI mock data. In the CORE contours, samples are coloured according to the value of H_0 .

to keep the BAO angular scale fixed, but this requires $\theta_s(z_{\text{dec}})$ to vary. The right plot in figure 5 illustrates, in an alternative way to the right plot of figure 4, how the combination of the two data sets can improve neutrino mass bounds.

Finally, we expect, as a secondary indirect effect, that the correlation between M_ν and $(A_s, \tau_{\text{reio}})$ will be more noticeable in a combined analysis of CMB and BAO than for CMB alone. In section 2.3, we mentioned in points 3 and 4 that the impact of M_ν on CMB lensing could be compensated in two ways: by increasing either $(A_s, \tau_{\text{reio}})$ (point 3) or ω_{cdm} (point 4). We explained why the former option is favoured with CMB data alone. Since we just argued that BAO data can reduce the degeneracy between neutrino masses and ω_{cdm} , the latter option is more relevant when the data are combined with each other. Indeed, we will see a small correlation between $(M_\nu, \tau_{\text{reio}})$ in the combined results presented in section 5, one that was hardly noticeable with CMB alone. Of course, this degeneracy is not perfect, and extends only up to the point at which τ_{reio} becomes too large to be compatible with CMB polarisation data.

4 Effect of neutrino mass on Large Scale Structure observables

4.1 Cosmic shear and galaxy clustering spectrum

The Euclid satellite, whose launch is scheduled for 2020, will provide the most accurate ever galaxy redshift survey, measuring cosmological observables, such as cosmic shear and galaxy clustering, with 1% accuracy. Euclid data will certainly lead to a major breakthrough in precision cosmology thanks to very precise low redshift measurement which will break the CMB degeneracies among cosmological parameters (see references [6, 9, 12, 13, 21, 27, 28, 35]). Here we use the information extracted from the cosmic shear power spectrum projected in angular harmonics (2D) and the galaxy clustering power spectrum (3D). Both observable are related to the non-linear matter power spectrum depending on wavenumber and redshift, $P_m(k, z)$. In our forecasts, we estimate this quantity using the HALOFIT algorithm, updated by [58] and also by [16] for the effect of neutrino masses, as implemented in CLASS v2.5.0.

Cosmic shear. The cosmic shear auto and cross correlation angular power spectrum in the i

and j redshift bins is given in the Limber approximation by:

$$C_\ell^{ij} = H_0^4 \int_0^\infty \frac{dz}{H(z)} W_i(z) W_j(z) P_m \left(k = \frac{l}{r(z)}, z \right), \quad (4.1)$$

where the window functions are given by

$$W_i(z) = \frac{3}{2} \Omega_m (1+z) \int_0^\infty dz_s \frac{n_i(z_s) (r(z_s) - r(z))}{r(z_s)}, \quad (4.2)$$

and the number of galaxies per steradian in the i bin is given by

$$n_i(z) = \frac{\int_{z_i^{\min}}^{z_i^{\max}} dn/dz \mathcal{P}(z, z_{\text{ph}}) dz_{\text{ph}}}{\int_0^\infty dn/dz \mathcal{P}(z, z_{\text{ph}}) dz_{\text{ph}}}$$

with $\mathcal{P}(z, z_{\text{ph}})$ being the error function

$$\mathcal{P}(z, z_{\text{ph}}) = \frac{1}{\sqrt{2\pi\sigma_{\text{ph}}^2}} \exp \left[-\frac{1}{2} \left(\frac{z - z_{\text{ph}}}{\sigma_{\text{ph}}} \right)^2 \right].$$

We use the Euclid prescription for the galaxy surface density

$$dn/dz = z^2 \exp \left[-(z/z_0)^{1.5} \right]$$

with $z_{\text{mean}} = 1.412z_0$. Finally we consider a photometric redshift error $\sigma_{\text{ph}} = 0.05(1+z)$, sky fraction $f_{\text{sky}} = 0.3636$, mean internal ellipticity 0.22 and total number of observed galaxies 30 per arcmin².

Galaxy clustering. For galaxy clustering the observed power spectrum reads:

$$P(k_{\text{ref}}, \mu, z) = \frac{D_A(z)_{\text{ref}}^2 H(z)}{D_A(z)_{\text{ref}}^2 H(z)_{\text{ref}}} b(z)^2 [1 + \beta(z, k(k_{\text{ref}}, \mu, z)) \mu^2]^2 \times P_m(k(k_{\text{ref}}, \mu, z)) e^{-k(k_{\text{ref}}, \mu, z)^2, z) \mu^2 \sigma_r^2},$$

where μ is the cosine of the angle between the line of sight and the wavenumber in the reference cosmology (ref) k_{ref} , k is the wavenumber in the true cosmology and it is defined as a function of k_{ref}

$$k^2 = \left(\frac{(1 - \mu^2) D_A(z)_{\text{ref}}^2}{D_A(z)_{\text{ref}}^2} + \frac{\mu^2 H(z)^2}{H(z)_{\text{ref}}^2} \right) k_{\text{ref}}^2.$$

The factor $[D_A(z)_{\text{ref}}^2 H(z)] / [D_A(z)_{\text{ref}}^2 H(z)_{\text{ref}}]$ encodes the geometrical distortions related to the Alcock-Paczynski effect. The bias can be written as $b = \sqrt{(1+z)}$, β encodes the redshift space distortions

$$\beta(k, z) = \frac{1}{2b(z)} \frac{d \ln P_m(k, z)}{d \ln a},$$

and finally the spectroscopic redshift error is $\sigma_r = dr(z)/dz \sigma_z$.

Both the C_ℓ and the $P(k)$ provide information on a broad range of scales, therefore, given the same survey sensitivity, they are more efficient than BAO in constraining cosmological parameters; however, for the very same reason, they are more prone to systematic effects such as residual errors in the estimate of non-linear corrections, non-linear light-to-mass bias or redshift space distortions (see e.g. [34, 54]). For that reason, some authors include in

their forecasts a theoretical error on the observable power spectrum, increasing above a given redshift-dependent scale of non-linearity (see [9], or [10] for a more refined treatment). Here we stick to the more common approach consisting in cutting the data at some k_{\max} in Fourier space and ℓ_{\max} in harmonic space. For galaxy clustering, the observational error decreases when k increases, so the choice of k_{\max} crucially impacts the results. Taking a too high value of k_{\max} would amount in including a lot of extra information with a very small error bar, while in reality, uncertainties on non-linear corrections could be larger than observational errors. In what follows, we will cut the observable $P(k_{\text{ref}}, \mu, z)$ at $k_{\max} = 0.2 h/\text{Mpc}$ for all redshifts. For cosmic shear, the choice of ℓ_{\max} is also important, although the error bar does not decrease indefinitely with ℓ due to the finite angular resolution of the shear maps. In our forecasts, we perform a conservative cut at $\ell_{\max} = 600$, corresponding to wavenumbers still in the mildly non-linear regime even for the highest redshift bins. When performing the integral over wavenumbers in equation (4.1), we keep up to $k_{\max} = 9 h/\text{Mpc}$, but the weight of wavenumbers above $0.2 h/\text{Mpc}$ is small, since they only contribute to the tail of the integrand in (4.1).

4.2 Degeneracies between M_ν and other parameters

In figure 6 and 7 we show the relative error in the shear power spectrum and in the galaxy power spectrum. The observational errors are computed in the same way as in Ref. [9], using the survey specifications listed above. We will study the impact of increasing the summed neutrino mass on these observables: (1) when keeping the usual cosmological parameters fixed, (2) when tuning h at the same time in order to keep the same angular peak scale in the CMB, and (3) when playing with other parameters in order to minimize the impact of neutrino mass on LSS observables. The discussion in (2) and (3) is relevant for understanding the degeneracy between M_ν and other parameters when fitting CMB+LSS data (2) or LSS data alone (3).

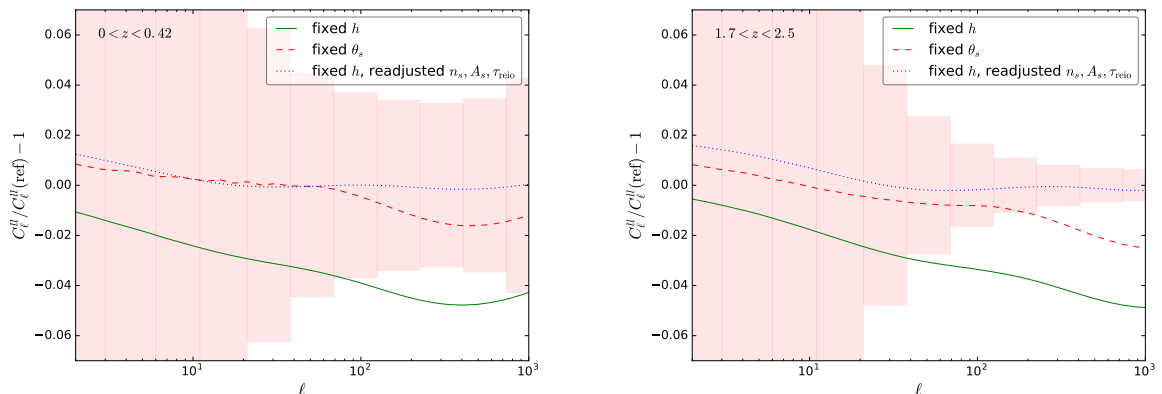


Figure 6. Relative error on the galaxy lensing C_ℓ^{ll} in the first redshift bin ($0 < z < 0.42$, left panel) and in the tenth redshift bin ($1.7 < z < 2.5$, right panel). Here the redshift range is $0 < z < 2.5$ and is divided in ten equi-populated redshift bins. The light pink rectangles refers to the observational error. Green solid line and red dashed lines are the same as in figure 1, i.e. higher M_ν with fixed h (green solid line) and higher M_ν with fixed θ_s and varying h (red dashed line). The blue dotted line, besides the higher M_ν with fixed h , also implies an increase of n_s by 0.4% and of A_s by 3% (and consistently an increase of τ_{reio}).

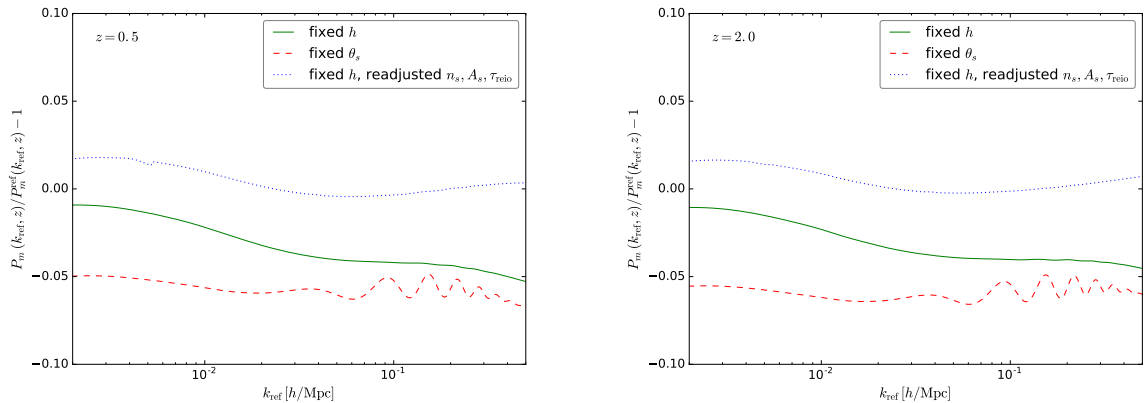


Figure 7. Relative error on the matter power spectrum $P_m(k)$ perpendicular to the line of sight at redshift $z = 0.5$ (left panel) and $z = 2$ (right panel). The light pink shaded area refers to the observational error, including cosmic variance. Here the redshift range is $0.5 < z < 2$ and is divided in 16 redshift bins. The line color/style - model correspondence is the same as in figure 6. However here the variation of A_s is 4% (blue dotted line).

1. *Neutrino mass effects with all standard cosmological parameters fixed.* As in the previous sections, we start by increasing the summed neutrino mass from $M_\nu = 0.06$ eV to $M_\nu = 0.15$ eV, keeping all the other cosmological parameters $\{\omega_b, \omega_{\text{cdm}}, h, n_s, A_s, \}$ fixed (green solid line). Note that in most of the literature, the effect of neutrino masses on the matter power spectrum is discussed precisely in that way. One reason is that fixing $\{\omega_b, \omega_{\text{cdm}}, n_s, A_s, \}$ amounts in keeping the same “early cosmological evolution” until the time of the neutrino non-relativistic transition. The choice to fix also h is mainly a matter of simplicity.

As expected, the larger M_ν induces a relative suppression of power on small scales compared to large scales, visible both in the shear and in the galaxy power spectrum. To be precise, in the redshift range surveyed by Euclid, $0 < z < 2.5$, neutrinos with a mass $M_\nu > 0.05$ eV are already well inside the non-relativistic regime, thus, the spectrum is suppressed on scales smaller than the free-streaming scale $k > k_{\text{fs}}$ respect to larger scales $k < k_{\text{fs}}$. In the redshift range of interest $0 < z < 2.5$ the free streaming wavenumber spans the range $[0.0077 - 0.0041]h\text{Mpc}^{-1}$ ($[0.0192 - 0.0103]h\text{Mpc}^{-1}$) for $M_\nu = 0.06$ eV ($M_\nu = 0.15$ eV)⁹. The suppression in power makes both the C_ℓ^{ij} and the $P(k)$ directly sensitive to the neutrino mass sum, while this was not the case for the purely geometrical information encoded in BAO measures.

This sensitivity is reinforced by non-linear effects which are well visible on figures 6 and 7. In the shear spectrum of figure 6, in absence of non-linear corrections, the green curve would be almost constant for $\ell > 100$. Non-linear gravitational clustering produced a characteristic “spoon shape” or dip [16]. The minimum of the dip is seen at $\ell \sim 40$ in the first redshift bin and $\ell \sim 1000$ in the last one. In figure 7, non-linear effects are responsible for the further decrease of the green curve for $k \geq 0.1 h/\text{Mpc}$.

2. *Neutrino mass effects with h varied to keep the CMB angular scales fixed.* The second

⁹The free streaming length depends on the mass of each neutrino rather than on the sum. Here we have assumed three massive degenerate neutrinos.

part of the discussion consists in increasing M_ν by the same amount, while varying h like in section 2.3, in such way keeping a constant angular diameter distance to recombination, constant sound horizon angular scale, and constant damping angular scale (red dashed line). As we have seen in Section 2.3 this procedure leads to the well known (M_ν, h) CMB degeneracy.

We showed that this degeneracy is broken by BAO data, because the lower value of h increases the angular diameter distance at low redshift (see Section 3). This conclusion is valid also for galaxy $P(k)$ and shear C_ℓ , since the red dashed residuals in figures 6, 7 are well outside the observational error bars. For clarity, we should explain the shape of these red dashed lines, which is slightly counter-intuitive.

In the case of galaxy clustering, the higher value of M_ν and lower value of h lead to an almost constant suppression of power on every scale, plus some wiggles on small scales (see figure 7). This may sound surprising since we are used to seeing more suppression on small scales when increasing the neutrino mass. This is true for fixed h , but here we are decreasing the Hubble rate at the same time. In order to understand the observed behaviour, we have to elaborate on the matter power spectrum P_m entering equation 4.1. An analytic study of the linear power spectrum expressed in units of $(\text{Mpc}/h)^3$ as a function of k in units of h/Mpc shows that at any given redshift, the large-scale branch ($k \ll k_{\text{eq}}$) depends only on a factor $(g(\Omega_m, z)/\Omega_m)^2$ coming from the Poisson equation and from the behavior of matter perturbations during Λ domination¹⁰. When reducing h , we increase this factor and suppress the large-scale power spectrum. The small-scale branch of the matter power spectrum is instead suppressed by massive neutrino free-streaming, coincidentally by roughly the same amount as the large-scale branch. This explains the almost constant suppression of power in the galaxy clustering spectrum (red dashed line, figure 7).

The situation is a bit different for the galaxy lensing spectrum C_ℓ (red dashed line, figure 6) which probes metric fluctuations instead of matter fluctuations. Thus it does not have the same dependence on Ω_m coming from the Poisson equation, and indeed the factor Ω_m^{-2} discussed in the previous paragraph is exactly cancelled by a factor Ω_m^2 that appears in equation 4.1 when replacing the window functions with equation 4.2. As a result the large-scale branch of the C_l 's depend on $g(\Omega_m, z)^2$ only and slightly increases when we decrease h . The small-scale branch remains nearly constant due to the antagonist effects of neutrino free-streaming and of the increase in Ω_m , but the neutrino effect wins takes over on non-linear scales.

Finally, by comparing the right panel of figure 6 with the left one, we can see that the tomographic information is crucial in breaking the (M_ν, h) degeneracy: Indeed the relative error induced by a larger M_ν and a smaller h is within the limit of the observational error in the first redshift bin, but not in the tenth redshift bin. The ability of galaxy lensing and clustering to lift the (M_ν, h) degeneracy is confirmed in the upper right panel of figure 9: galaxy clustering does not show any significant correlation between the neutrino mass sum and the Hubble constant, while in the case of cosmic shear the degeneracy between H_0 and M_ν seems to be even mildly positive, in stark contrast with the steep negative correlation encoded in CMB measurements.

¹⁰see e.g. [43], equation (6.39). $g(\Omega_m, z) \leq 1$ is related to the decrease of matter perturbations during Λ domination.

3. *Degeneracy between M_ν and other parameters from Large Scale Structure data alone.* Finally we increase M_ν , keeping fixed h , and, at the same time, we vary the primordial power spectrum parameters, the amplitude A_s and the index n_s (blue dotted line). It is clear from figures 6 and 7 that this procedure can almost cancel the effect induced by a larger M_ν both in the shear C_ℓ and in the galaxy $P(k)$, leading to a new degeneracy.

The reason of this degeneracy can be better understood if we have a closer look at the matter power spectrum in neutrino cosmologies and at the primordial power spectrum of scalar perturbations. Considering that the primordial power spectrum of scalar perturbations is given by

$$\frac{k^3 \mathcal{P}_{\mathcal{R}}(k)}{2\pi^2} = A_s \left(\frac{k}{k_0} \right)^{n_s-1}, \quad (4.3)$$

the matter power spectrum P_m can be written as

$$P_m(k, z) \propto A_s \left(\frac{k}{k_0} \right)^{n_s-1} T(k, z)^2 \quad (4.4)$$

where $T(k, z)$ is the time and scale dependent linear transfer function of matter density fluctuations (not separable in the case of massive neutrinos). As we have already

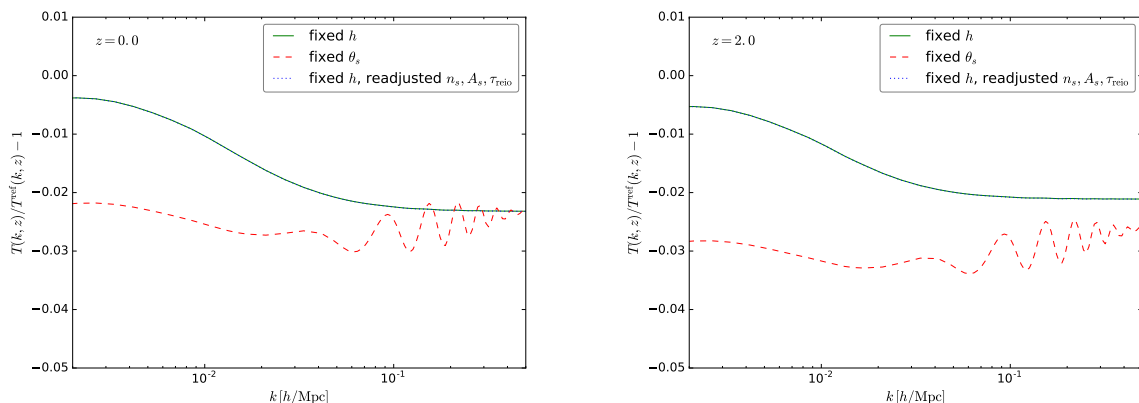


Figure 8. Relative error on the linear transfer function $T(k)$ at redshift $z = 0$ (left panel) and $z = 2$ (right panel). The line color/style - model correspondence is the same as in figure 7.

explained, neutrinos induce a relative suppression of power on scales $k > k_{\text{fs}}$; this suppression is encoded in the transfer function $T(k, z)$ of equation 4.4. In figure 8 we show how $T(k, z)$ is suppressed by a larger neutrino mass sum on $k > k_{\text{fs}}$ at redshift $z = 0$ and $z = 2$. Changing (n_s, A_s) affects only the primordial power spectrum, while leaving $T(k, z)$ unchanged, therefore the blue dotted line overlaps to the green solid line. The key point is that if, besides increasing M_ν , we decrease h to keep θ_s fixed (red dashed line), then the suppression of $T(k, z)$ extends to $k < k_{\text{fs}}$. This explains why the scale dependent suppression induced by an increase in M_ν cannot be compensated by a lower value of h .

However, if we look at equation 4.4 it is clear that a red tilt of the primordial power spectrum, combined with a smaller normalization, can mimic the same effect of a larger neutrino mass, reducing power on small scales respect to large scales.

Left and right bottom panels of figure 9 show the degeneracies between M_ν and (n_s, A_s) . We can see that the degeneracy between M_ν and n_s is positive in galaxy lensing, as expected from the discussion above, while it is negative in CMB, as explained at the end of section 2.3, and mildly negative in galaxy clustering. The reason why this positive (M_ν, n_s) correlations can be captured by cosmic shear, but not by galaxy correlation data, is related to the window function. Indeed, since the window function (equation 4.2) for each redshift bin is given by the integral over the line of sight, the C_ℓ^{ij} of equation 4.1 receive contribution from a larger range of scales. Therefore, being sensitive to a longer lever arm in k space, cosmic shear will be particularly sensitive to scale dependent variations of the power spectrum.

The final effect is that galaxy lensing will compensate for an increase of M_ν by increasing n_s , which compensate the small scale suppression, and, at the same time, also increasing A_s , so that the increase of n_s will not reduce power on large scales.

In the case of galaxy clustering, the suppression induced by the increase of M_ν will be compensated by a larger A_s , so the main correlation will be the one between M_ν and A_s .

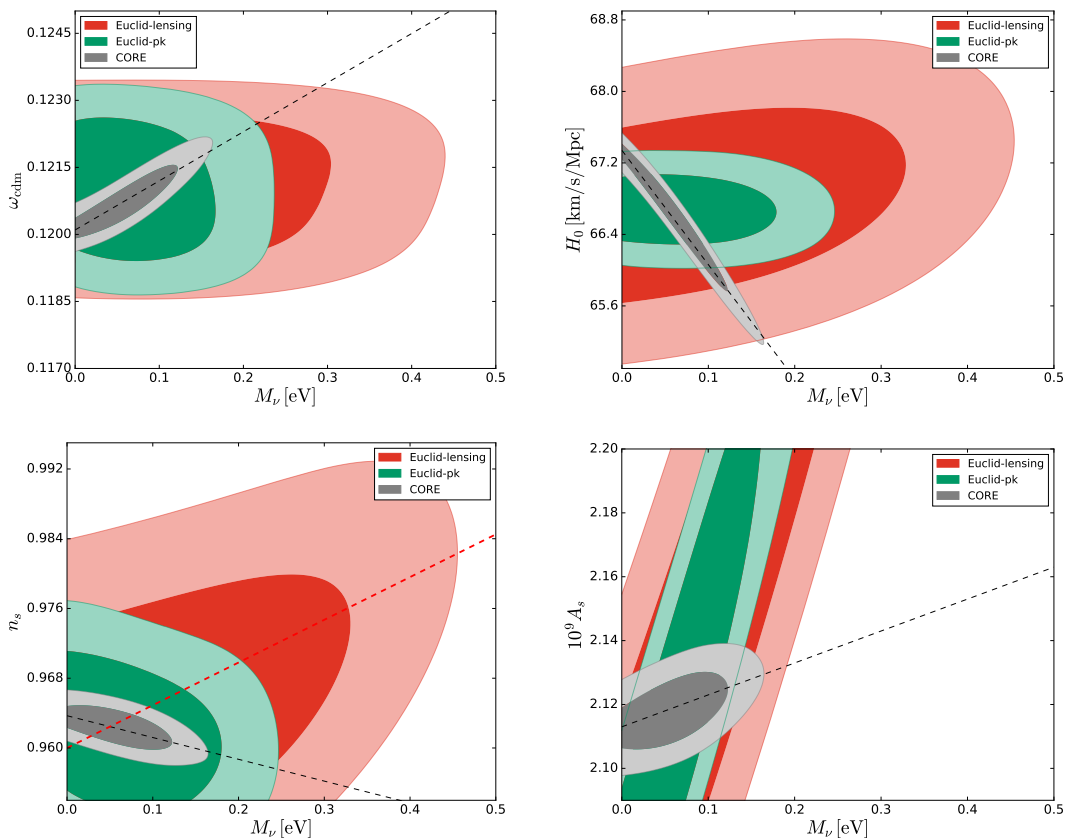


Figure 9. Marginalized one- and two- σ contours in the plane $(\omega_{\text{cdm}}, M_\nu)$ (upper left panel), (H_0, M_ν) (upper right panel), (A_s, M_ν) (bottom left panel), (A_s, M_ν) (bottom right panel). The black dashed lines show the degeneracies encoded in CMB data, the red dashed line in the bottom left panel represents the positive correlation between M_ν and n_s arising from cosmic shear.

Figure 9 depicts the marginalized one- and two- σ contours in the plane $(\omega_{\text{cdm}}, M_\nu)$ (upper left panel), (H_0, M_ν) (upper right panel), (n_s, M_ν) (bottom left panel), (A_s, M_ν) (bottom right panel). The CORE only contours are the same as in figure 4. The Euclid related contours have been obtained through an MCMC forecast including either galaxy clustering or cosmic shear, following the same procedure as in Ref. [9] and the specifications of section 4.1. Here we keep ω_b fixed, because it is pinned down by CMB experiments, and τ_{reio} , which does not affect galaxy clustering and shear observables.

Besides proving the points that we have discussed above, Figure 9 shows that the degeneracy between M_ν and A_s is the dominant one for LSS data. This will play an important role when studying joint CMB+LSS constraints in the next section. Note also that in figure 9, all Euclid-based contours are rather wide compared to the CORE ones. One should however remember that they are marginalised over the remaining three parameters (e.g. the (M_ν, H_0) contours are marginalised over ω_{cdm} , A_s and n_s). When combining CMB and LSS data, many parameter combinations will be fixed, and we will see that Euclid data play a crucial role in reducing parameter degeneracies, beyond what could be expected by looking at the LSS-only contours in Figure 9.

5 Joint Analysis Results

5.1 Combination of CMB, BAO and galaxy shear/correlation data

In this section we will present the results of our Markov Chain Monte Carlo forecast of the sensitivity of future CMB, BAO and LSS experiments to the cosmological parameters described in Section 2, in particular to the neutrino mass sum. As already mentioned in Section 2.3, our MCMC forecast will be performed using the MONTEPYTHON code¹¹ [8], interfaced with the Boltzmann solver CLASS¹² [17, 42, 45]. As argued in section 4.1, the result of such an exercise depends crucially on the choice of cut-off scales k_{max} and ℓ_{max} . We choose $k_{\text{max}} = 0.2 h/\text{Mpc}$ for galaxy correlation and $\ell_{\text{max}} = 600$ for cosmic shear, arguing that in that way our results only require a precise modelling of non-linear corrections up to mildly non-linear scales; still this choice is arbitrary, and different assumptions would lead to different parameter sensitivities.

	$\sigma(M_\nu)/[\text{meV}]$	$\sigma(\tau_{\text{reio}})$	$\sigma(10^9 A_s)$	$\sigma(n_s)$	$\sigma(\omega_{\text{cdm}})$	$\sigma(h)$
CORE	42	0.0020	0.0084	0.0018	0.00052	0.0052
CORE+DESI	19	0.0020	0.0080	0.0014	0.00026	0.0022
CORE+DESI+Euclid	7	0.0019	0.0075	0.0014	0.00015	0.0007
CORE+DESI+Euclid+21cm	5	—	0.0039	0.0013	0.00012	0.0007

Table 1. Expected 1σ sensitivity of CORE, CORE + DESI, CORE + DESI + Euclid and CORE + DESI + Euclid + “21cm-motivated τ_{reio} prior” to M_ν , τ_{reio} , $10^9 A_s$, n_s , ω_{cdm} and h .

In the first three lines of table 1 we report the expected sensitivity of CORE, CORE+DESI and CORE+DESI+Euclid to M_ν and other cosmological parameters playing a crucial role in our analysis of parameter degeneracies: τ_{reio} , $10^9 A_s$, n_s , ω_{cdm} and h (the last independent parameter, ω_b , is always very well constrained by CMB data alone). In figure 10 we plot the one dimensional posteriors and the one- and two- σ marginalized contours for the same parameters.

¹¹<http://baudren.github.io/montepython.html>

¹²<http://class-code.net>

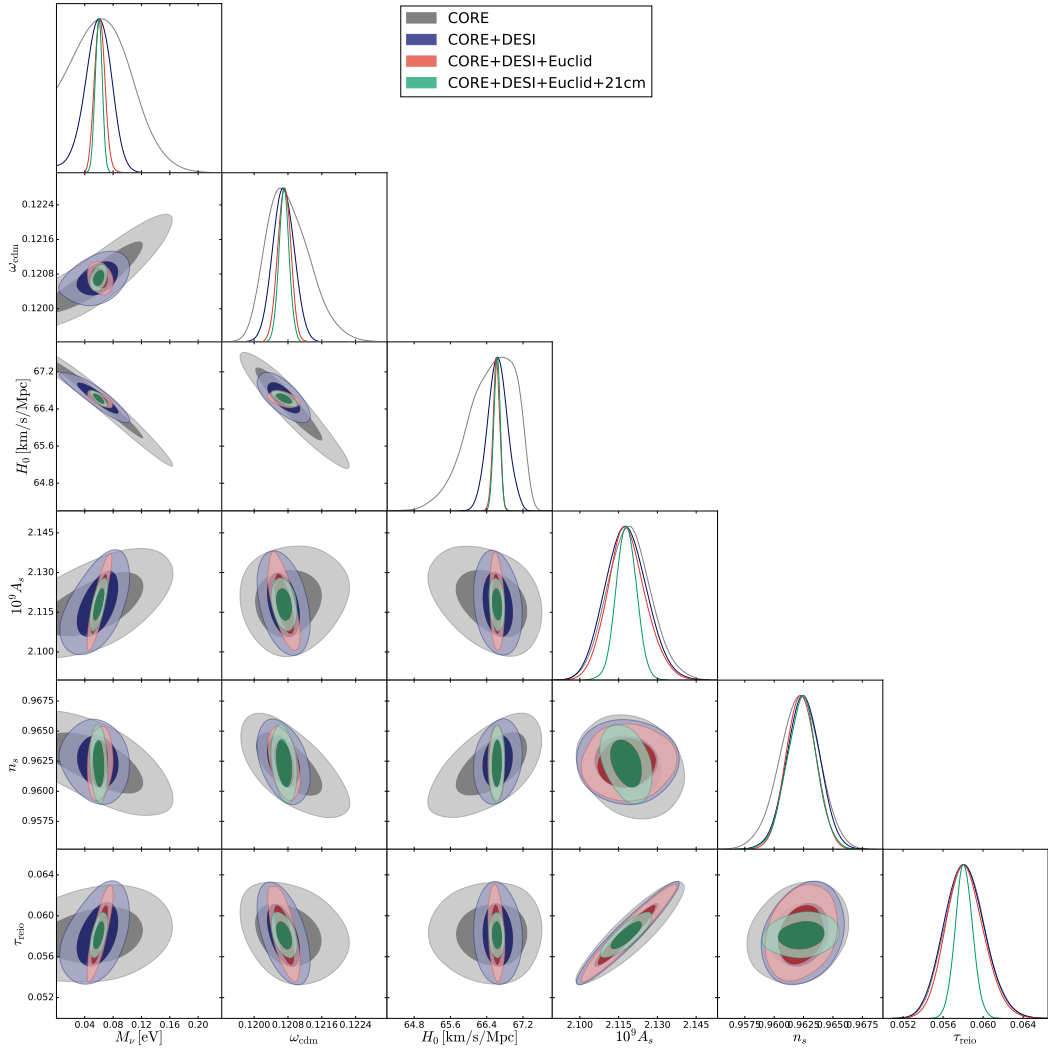


Figure 10. Marginalized one and two σ contours and one dimensional posteriors in the plane $(M_\nu, \omega_{\text{cdm}}, H_0, A_s, n_s, \tau_{\text{reio}})$ parameter space showing the expected sensitivity of various future experiments: CORE only (gray contours), CORE+DESI (blue contours), CORE+DESI+Euclid (red contours) and CORE+DESI+Euclid+21cm (green contours). The last independent parameter, ω_b , is always very well constrained by CMB data alone.

First of all we notice that the projected 1σ errors in table 1 and 1D distributions in figure 10 reflect the theoretical points we have discussed in the previous sections: both DESI and Euclid greatly improve the sensitivity to the neutrino mass sum, as well as ω_{cdm} and h . The uncertainty on the M_ν tightens by more than a factor two for CORE+DESI and a factor six for CORE+DESI+Euclid, compare to the CORE only sensitivity. That on ω_{cdm} tightens respectively by a factor two and four. The error on H_0 goes from 0.52 km/s/Mpc for CORE only, to 0.22 km/s/Mpc for CORE+DESI and 0.07 km/s/Mpc for CORE+DESI+Euclid. However once more we want to stress that in the case of DESI the improved sensitivity arises from reducing the degeneracy between H_0 and M_ν , while in the case of Euclid the longer lever arm of the shear data is specifically sensitive to the suppression of power at small scales induced by M_ν .

The first column of figure 10 shows all the degeneracies with respect to M_ν . The extended regions defining the positive correlation between $(M_\nu, \omega_{\text{cdm}})$ and (M_ν, H_0) in CORE are reduced with CORE+DESI, and even more when adding Euclid. The positive correlation with A_s becomes more and more steep with the inclusion of DESI and Euclid. The negative correlation with n_s is reduced by DESI and completely disappears thanks to Euclid. Finally the degeneracy with τ_{reio} , which is negligible in CORE, becomes a well defined positive correlation with DESI and even more clearly with Euclid, as a consequence of the increasingly important (M_ν, A_s) degeneracy, and of the fact that the CMB fixes the combination $A_s e^{-2\tau_{\text{reio}}}$.

In the top 2D plot of the second column and in the third column of figure 10, we can verify the ability of large scale structure measurements to break the degeneracies related to H_0 in models with a varying neutrino mass.

In the second panel of the second column of figure 10, it is interesting to notice the flipping of the degeneracy between ω_{cdm} and A_s : Indeed, while the two parameters have the same effect on CMB lensing (see point 3 and 4 of section 2.3), both contributing to reduce the relative error induced by a larger M_ν , large scale structure tend to keep ω_{cdm} close to the fiducial value and compensate the higher M_ν varying A_s , directly in the case of galaxy shear and clustering, indirectly by breaking the degeneracy between H_0 and Ω_m in the case of DESI. An analogous effect is responsible for lifting the degeneracy between ω_{cdm} and n_s in the third panel of the second column.

To further improve measurements of the neutrino mass with cosmological data, one should try to add independent constraints on the parameters that remain most correlated with M_ν in the CMB+BAO+LSS contours: these are H_0 , A_s and τ_{reio} . It was previously noticed in Ref. [47] that 21cm surveys could improve the determination of the optical depth to reionization, and thus of the summed neutrino mass. In the next section we will further investigate this possibility.

5.2 Adding 21cm surveys

In the near future, many experimental efforts will be devoted to measuring precisely the epoch of recombination (EoR), mostly through the 21 cm line created by the hyperfine transition of the Hydrogen atom¹³, including the value of τ_{reio} . In general, details of the EoR are strongly connected to fundamental questions in cosmology and astrophysics. It could teach us about many properties of the first galaxies and quasars, such as the time at which they form, how did the formation of very metal-poor stars proceed, as well as whether first galaxies were indeed the only re-ionizing source.

However, these experiments can also have great implications for neutrino physics in cosmology. Indeed, the independent measure of the epoch of reionization by 21cm surveys will break the degeneracy between A_s and τ_{reio} [47, 59]. Compensating the variation of the neutrino mass with a variation of A_s in CMB lensing or in Large Scale Structure observables will no longer be possible.

To assess the impact of 21cm surveys on the improvement of the determination of the neutrino mass, we have performed a run combining all previous experiments, namely CORE+DESI+Euclid, adding a gaussian prior on the value of τ_{reio} as it could be measured with HERA or SKA sensitivity $\sigma(\tau_{\text{reio}}) = 0.01$ [47, 57]. Note that by doing so we are

¹³e.g. PAPER 64: <http://eor.berkeley.edu>, 21CMA: <http://21cma.bao.ac.cn>, MWA: <http://www.mwatelescope.org>, LOFAR: <http://www.lofar.org>, HERA: <http://reionization.org> or SKA: <http://www.skatelescope.org>.

conservative, since 21cm surveys will not only yield the evolution of the mean free electron fraction $x_e(z)$ (and thus the optical depth τ_{reio}), but also the power spectrum of the 21cm signal at different redshift $P_{21}(k, z)$, related to variations along the line of sights of the free electron fraction $x_e(\hat{n}, z)$ [49]. We are therefore using the minimal amount of information that one can extract from these experiments, and one could go beyond following e.g. the procedure of Ref. [47].

The results of our MCMC forecast, summarized by the last line of table 1 and the green contours in figure 10, typically show that the sensitivity on the neutrino mass could almost double thanks to 21cm data, going from $\sigma(M_\nu) = 7$ meV for CORE+DESI+Euclid to 5 meV. This result is consistent with that of Ref. [47]. Thus, even if nature has chosen the summed neutrino mass to be close to the lower limit of the normal hierarchy, $M_\nu = 60$ meV, the joint analysis of CORE+DESI+Euclid+21cm will provide a detection at more than 10σ .

6 Conclusions

The foundations of a new era in precision cosmology are based on two cornerstones: the high sensitivity of future CMB and galaxy survey experiments, and a deep understanding of the physics governing the processes of recombination and structure formation. The extreme accuracy of future data will offer the opportunity to constrain particle physics with cosmology, exceeding in many cases the precision of laboratory experiments. However, in order to exploit the new data, cosmologists will need an accurate enough theoretical model taking into account the underlying physics.

Neutrinos provide an excellent example of how the sensitivity of future cosmological surveys may lead to such an important result as the summed neutrino mass detection, even when uncertainties on the details of the cosmological model are marginalised over.

In this paper we have provided a careful discussion of the physical effects induced by massive neutrinos and their impact on cosmological observables, as they will appear in the data analysis of the next generation of cosmological experiments. We have shown how the unique nature of light neutrinos, being relativistic until very late times and behaving as a matter component after the non relativistic transition, makes possible to identify different signatures at different epochs of the cosmic history. Therefore the correlation between the summed neutrino mass and the other cosmological parameters changes, depending on the redshift range probed by the various data sets.

Our results on the sensitivity of future CMB-CORE and BAO-DESI experiments to the summed neutrino mass are consistent with the literature (see Refs. [4, 47]). Moreover the results of our forecasts including a Euclid-like survey prove the importance of cosmic shear and galaxy clustering as complementary probes. In particular we have shown how the longer lever arm of cosmic shear data will be able to flip the degeneracy between the summed neutrino mass and the primordial power spectrum index, leading to a very high sensitivity both on M_ν ($\sigma(M_\nu) = 7$ meV) and on n_s ($\sigma(n_s) = 0.0014$). We pointed out that the results of our Euclid cosmic shear + galaxy correlation forecasts depend very much on the choice of the cut-off scales introduced to remove information and systematics coming from the deep non-linear regime. Nevertheless they are again compatible with previously published results. For instance, Ref. [35] found $\sigma(M_\nu) = 11$ meV for Planck + Euclid cosmic shear / galaxy correlation, without CORE and DESI-BAO data. Ref. [8] found a larger error, close to 20 meV, but for Planck + Euclid cosmic shear or Planck + Euclid galaxy correlation, not

trying to combine the two LSS probes together (and using a very conservative treatment of theoretical errors).

Anyhow, the main goal of this study was not to present a new set of forecasts, but to discuss the details of physical effects and parameter degeneracies involving neutrino masses. In particular, we clarified the reason for which an unexpected degeneracy between the neutrino mass sum and the optical depth at reionization will appear in the analysis of future high precision galaxy surveys, as already pointed out e.g. in [4, 47]. We showed that this degeneracy is not present in a CMB-only analysis, because the neutrino mass effects on CMB lensing can be compensated by playing with h and ω_{cdm} in a better way than by adjusting $(A_s, \tau_{\text{reio}})$. However, the former degeneracy is lifted once BAO and LSS low redshift measurements are taken into account. Moreover, we demonstrated that the LSS data introduce a strong correlation between M_ν and A_s , which finally leads to a clear $(M_\nu, \tau_{\text{reio}})$ degeneracy in the combined CMB+BAO+LSS analysis.

These conclusions clarify why further independent measurements of the optical depth will greatly benefit to the neutrino mass determination, as previously noticed by the authors of [47]. For instance, the results from the HERA or SKA 21cm surveys will provide an independent constraint on τ_{reio} , thus breaking this degeneracy. Our results indicate that this could half the error on M_ν with respect to the CMB+BAO+LSS case, leading to a robust detection of the summed neutrino mass at more than 10σ for CORE+DESI+Euclid+HERA or SKA.

In conclusion, the remarkable complementarity of future different cosmological data will lead to extremely accurate constraints on the neutrino mass sum and, possibly, on other neutrino properties, answering some of the still open questions of modern physics.

Acknowledgement

JL acknowledges extremely useful discussions with A. Challinor. VP is supported by the ‘‘Investissements d’avenir, Labex ENIGMASS’’, of the French ANR. This work has been done thanks to the facilities offered by the RWTH High Performance Computing cluster, and the Université Savoie Mont Blanc MUST computing center.

References

- [1] P. A. R. Ade et al. Planck 2015 results. XIII. Cosmological parameters. *Astron. Astrophys.*, 594:A13, 2016.
- [2] N. Aghanim et al. Planck intermediate results. XLVI. Reduction of large-scale systematic effects in HFI polarization maps and estimation of the reionization optical depth. 2016.
- [3] Yacine Ali-Haïmoud and Simeon Bird. An efficient implementation of massive neutrinos in non-linear structure formation simulations. *Mon. Not. Roy. Astron. Soc.*, 428:3375–3389, 2012.
- [4] Rupert Allison, Paul Caucal, Erminia Calabrese, Joanna Dunkley, and Thibaut Louis. Towards a cosmological neutrino mass detection. *Phys. Rev.*, D92:123535, 2015.
- [5] Lauren Anderson et al. The clustering of galaxies in the sdss-iii baryon oscillation spectroscopic survey: Baryon acoustic oscillations in the data release 10 and 11 galaxy samples. *Mon. Not. Roy. Astron. Soc.*, 441:24–62, 2014.
- [6] Maria Archidiacono, Tobias Basse, Jan Hamann, Steen Hannestad, Georg Raffelt, and Yvonne Y. Y. Wong. Future cosmological sensitivity for hot dark matter axions. *JCAP*, 1505(05):050, 2015.

- [7] Maria Archidiacono and Steen Hannestad. Efficient calculation of cosmological neutrino clustering in the non-linear regime. *JCAP*, 1606(06):018, 2016.
- [8] Benjamin Audren, Julien Lesgourgues, Karim Benabed, and Simon Prunet. Conservative Constraints on Early Cosmology: an illustration of the Monte Python cosmological parameter inference code. *JCAP*, 1302:001, 2013.
- [9] Benjamin Audren, Julien Lesgourgues, Simeon Bird, Martin G. Haehnelt, and Matteo Viel. Neutrino masses and cosmological parameters from a Euclid-like survey: Markov Chain Monte Carlo forecasts including theoretical errors. *JCAP*, 1301:026, 2013.
- [10] Tobias Baldauf, Mehrdad Mirbabayi, Marko Simonovi, and Matias Zaldarriaga. LSS constraints with controlled theoretical uncertainties. 2016.
- [11] Sergei Bashinsky and Uros Seljak. Neutrino perturbations in CMB anisotropy and matter clustering. *Phys. Rev.*, D69:083002, 2004.
- [12] Tobias Basse, Ole Eggers Bjaelde, Jan Hamann, Steen Hannestad, and Yvonne Y. Y. Wong. Dark energy properties from large future galaxy surveys. *JCAP*, 1405:021, 2014.
- [13] Tobias Basse, Jan Hamann, Steen Hannestad, and Yvonne Y. Y. Wong. Getting leverage on inflation with a large photometric redshift survey. *JCAP*, 1506(06):042, 2015.
- [14] Florian Beutler, Chris Blake, Matthew Colless, D. Heath Jones, Lister Staveley-Smith, et al. The 6df galaxy survey: Baryon acoustic oscillations and the local hubble constant. *Mon.Not.Roy.Astron.Soc.*, 416:3017–3032, 2011.
- [15] Florian Beutler et al. The clustering of galaxies in the completed SDSS-III Baryon Oscillation Spectroscopic Survey: Baryon Acoustic Oscillations in Fourier-space. *Submitted to: Mon. Not. Roy. Astron. Soc.*, 2016.
- [16] Simeon Bird, Matteo Viel, and Martin G. Haehnelt. Massive Neutrinos and the Non-linear Matter Power Spectrum. *Mon. Not. Roy. Astron. Soc.*, 420:2551–2561, 2012.
- [17] Diego Blas, Julien Lesgourgues, and Thomas Tram. The Cosmic Linear Anisotropy Solving System (CLASS) II: Approximation schemes. *JCAP*, 1107:034, 2011.
- [18] F. R. Bouchet et al. CORe (Cosmic Origins Explorer) A White Paper. 2011.
- [19] Jacob Brandbyge, Steen Hannestad, Troels Haugbllle, and Bjarne Thomsen. The Effect of Thermal Neutrino Motion on the Non-linear Cosmological Matter Power Spectrum. *JCAP*, 0808:020, 2008.
- [20] Jacob Brandbyge, Steen Hannestad, Troels Haugbllle, and Yvonne Y. Y. Wong. Neutrinos in Non-linear Structure Formation - The Effect on Halo Properties. *JCAP*, 1009:014, 2010.
- [21] Carmelita Carbone, Licia Verde, Yun Wang, and Andrea Cimatti. Neutrino constraints from future nearly all-sky spectroscopic galaxy surveys. *JCAP*, 1103:030, 2011.
- [22] Emanuele Castorina, Carmelita Carbone, Julien Bel, Emiliano Sefusatti, and Klaus Dolag. DEMNUni: The clustering of large-scale structures in the presence of massive neutrinos. *JCAP*, 1507(07):043, 2015.
- [23] Antonio J. Cuesta, Viviana Niro, and Licia Verde. Neutrino mass limits: robust information from the power spectrum of galaxy surveys. *Phys. Dark Univ.*, 13:77–86, 2016.
- [24] E. De Valentino and others [CORE collaboration]. *in preparation*.
- [25] G. De Zotti et al. Exploring Cosmic Origins with CORE: Extragalactic sources in Cosmic Microwave Background maps. 2016.
- [26] J. Delabrouille and others [CORE collaboration]. *in preparation*.
- [27] Enea Di Dio, Francesco Montanari, Ruth Durrer, and Julien Lesgourgues. Cosmological Parameter Estimation with Large Scale Structure Observations. *JCAP*, 1401:042, 2014.

- [28] Enea Di Dio, Francesco Montanari, Julien Lesgourgues, and Ruth Durrer. The CLASSgal code for Relativistic Cosmological Large Scale Structure. *JCAP*, 1311:044, 2013.
- [29] He Dupuy and Francis Bernardeau. On the importance of nonlinear couplings in large-scale neutrino streams. *JCAP*, 1508(08):053, 2015.
- [30] Andreu Font-Ribera et al. Desi and other dark energy experiments in the era of neutrino mass measurements. *JCAP*, 1405:023, 2014.
- [31] Florian Frer and Yvonne Y. Y. Wong. Higher-order massive neutrino perturbations in large-scale structure. *JCAP*, 1503(03):046, 2015.
- [32] Elena Giusarma, Martina Gerbino, Olga Mena, Sunny Vagnozzi, Shirley Ho, and Katherine Freese. On the improvement of cosmological neutrino mass bounds. 2016.
- [33] M. C. Gonzalez-Garcia, Michele Maltoni, and Thomas Schwetz. Global Analyses of Neutrino Oscillation Experiments. *Nucl. Phys.*, B908:199–217, 2016.
- [34] Jan Hamann, Steen Hannestad, Julien Lesgourgues, Cornelius Rampf, and Yvonne Y. Y. Wong. Cosmological parameters from large scale structure - geometric versus shape information. *JCAP*, 1007:022, 2010.
- [35] Jan Hamann, Steen Hannestad, and Yvonne Y. Y. Wong. Measuring neutrino masses with a future galaxy survey. *JCAP*, 1211:052, 2012.
- [36] Steen Hannestad. Neutrino physics from precision cosmology. *Prog. Part. Nucl. Phys.*, 65:185–208, 2010.
- [37] G. Hinshaw et al. Nine-Year Wilkinson Microwave Anisotropy Probe (WMAP) Observations: Cosmological Parameter Results. *Astrophys. J. Suppl.*, 208:19, 2013.
- [38] Ren Hlozek, David J. E. Marsh, Daniel Grin, Rupert Allison, Jo Dunkley, and Erminia Calabrese. Future CMB tests of dark matter: ultra-light axions and massive neutrinos. 2016.
- [39] Z. Hou et al. Constraints on Cosmology from the Cosmic Microwave Background Power Spectrum of the 2500 deg² SPT-SZ Survey. *Astrophys. J.*, 782:74, 2014.
- [40] Cullan Howlett, Antony Lewis, Alex Hall, and Anthony Challinor. CMB power spectrum parameter degeneracies in the era of precision cosmology. *JCAP*, 1204:027, 2012.
- [41] Wayne T. Hu. *Wandering in the Background: A CMB Explorer*. PhD thesis, UC, Berkeley, 1995.
- [42] Julien Lesgourgues. The Cosmic Linear Anisotropy Solving System (CLASS) I: Overview. 2011.
- [43] Julien Lesgourgues, Gianpiero Mangano, Gennaro Miele, and Sergio Pastor. *Neutrino cosmology*. Cambridge Univ. Press, Cambridge, 2013.
- [44] Julien Lesgourgues and Sergio Pastor. Neutrino mass from Cosmology. *Adv. High Energy Phys.*, 2012:608515, 2012.
- [45] Julien Lesgourgues and Thomas Tram. The Cosmic Linear Anisotropy Solving System (CLASS) IV: efficient implementation of non-cold relics. *JCAP*, 1109:032, 2011.
- [46] Antony Lewis and Anthony Challinor. Weak gravitational lensing of the cmb. *Phys. Rept.*, 429:1–65, 2006.
- [47] Adrian Liu, Jonathan R. Pritchard, Rupert Allison, Aaron R. Parsons, Uro Seljak, and Blake D. Sherwin. Eliminating the optical depth nuisance from the CMB with 21 cm cosmology. *Phys. Rev.*, D93(4):043013, 2016.
- [48] T. Matsumura et al. LiteBIRD: Mission Overview and Focal Plane Layout. *J. Low. Temp. Phys.*, 184(3-4):824–831, 2016.
- [49] Garrelt Mellema et al. Reionization and the Cosmic Dawn with the Square Kilometre Array.

- Exper. Astron.*, 36:235–318, 2013.
- [50] Takemi Okamoto and Wayne Hu. CMB lensing reconstruction on the full sky. *Phys. Rev.*, D67:083002, 2003.
 - [51] Nathalie Palanque-Delabrouille et al. Neutrino masses and cosmology with Lyman-alpha forest power spectrum. *JCAP*, 1511(11):011, 2015.
 - [52] Z. Pan, L. Knox, and M. White. Dependence of the Cosmic Microwave Background Lensing Power Spectrum on the Matter Density. *Mon. Not. Roy. Astron. Soc.*, 445(3):2941–2945, 2014.
 - [53] Laurence Perotto, Julien Lesgourgues, Steen Hannestad, Huitzu Tu, and Yvonne Y. Y. Wong. Probing cosmological parameters with the CMB: Forecasts from full Monte Carlo simulations. *JCAP*, 0610:013, 2006.
 - [54] Anais Rassat, Adam Amara, Luca Amendola, Francisco J. Castander, Thomas Kitching, Martin Kunz, Alexandre Refregier, Yun Wang, and Jochen Weller. Deconstructing Baryon Acoustic Oscillations: A Comparison of Methods. 2008.
 - [55] Adam G. Riess et al. A 2.4% Determination of the Local Value of the Hubble Constant. *Astrophys. J.*, 826(1):56, 2016.
 - [56] Ashley J. Ross, Lado Samushia, Cullan Howlett, Will J. Percival, Angela Burden, et al. The clustering of the sdss dr7 main galaxy sample i: A 4 per cent distance measure at $z=0.15$. *Mon. Not. Roy. Astron. Soc.*, 449(1):835–847, 2015.
 - [57] Mario G. Santos et al. Cosmology with a SKA HI intensity mapping survey. 2015.
 - [58] Ryuichi Takahashi, Masanori Sato, Takahiro Nishimichi, Atsushi Taruya, and Masamune Oguri. Revising the Halofit Model for the Nonlinear Matter Power Spectrum. *Astrophys. J.*, 761:152, 2012.
 - [59] Francisco Villaescusa-Navarro, Philip Bull, and Matteo Viel. Weighing neutrinos with cosmic neutral hydrogen. *Astrophys. J.*, 814(2):146, 2015.